Spring 2019

Computational fluid dynamics modeling of proppant static settling velocity in high viscosity friction reducers

Chen Yuan

Department:

COMPUTATIONAL FLUID DYNAMICS MODELING OF PROPPANT STATIC SETTLING VELOCITY IN HIGH VISCOSITY FRICTION REDUCERS

by

CHEN YUAN

A THESIS

Presented to the Faculty of the Graduate School of the

MISSOURI UNIVERSITY OF SCIENCE AND TECHNOLOGY

In Partial Fulfillment of the Requirements for the Degree

MASTER OF SCIENCE IN PETROLEUM ENGINEERING

2019

Approved by:

Dr. Abdulmohsin Imqam, Advisor
Dr. Shari Dunn-Norman
Dr. Ralph Flori

ABSTRACT

In the current petroleum fracturing industry, it is necessary to understand the downhole migration and settling velocity of the proppant. If we can master this information well, it will be a great help to obtain effective propped fracture conductivity. In order to study the transport of proppants in the well, we used laboratory experiments and computer numerical simulations to compare the results to get a meaningful conclusion. We spent a lot of time building models on a powerful computer and comparing the experimental conclusions. We finally decided to use computational fluid dynamics (CFD) as the simulation platform, discrete phase method (DPM) as the base model, and compare the simulation data with settling velocity experiment data to draw conclusions. Three cases were run and tested including fracture fluid type, proppant size, and fracture orientations. Results show a good integration between experimental results and simulation outputs. This work will help to provide a full understanding of the distinct changes of the mechanical characterization on the High Viscosity Friction Reducers (HVFRs). The findings provide an in-depth understanding of the behavior of HVFRs under confined effect, which could be used as guidance for fracture engineers to design and select better HVFR design.

ACKNOWLEDGMENTS

I would like to express my appreciation towards my advisor Dr. Abdulmohsin Imqam for providing me the opportunity of the research and teach me how to be a qualified master student and he always having faith in me.

Thanks to my committee members, Dr. Shari Dunn-Norman for always being friendly and open to discuss any problem and Dr. Ralph Flori for sparing all the possible time from his busy schedule.

Thanks to my parents. My parents make everything possible on me which I would never forget.

Especially I would like to thank Mohammed Ba Geri and Chao Zeng, not only we finished a ARMA conference paper together, but also thanks them for helping me on my research. Brotherhood always first.

A special thanks to B.J Services for their cooperation and assistance supporting this work as well as provide HVFRs and Linear gel samples. I also would like to acknowledge U.S. Silica for providing the proppant used in this paper.

TABLE OF CONTENTS

Page

LIST OF ILLUSTRATIONS

LIST OF TABLES

NOMENCLATURE

Symbol	Description
g	Gravitational Constant, 980 cm/s2
P^f	Fluid Density, gm/cm3
dp	Particle Diameter, cm
μ	Fluid Viscosity, poise
$\vec{u}$	The Velocity Vector
ρ	The Density of Fluid
P	The Static Pressure
$\vec{F}$	The General Body Force
ρ_a	Density of Air
ρ_w	Density of Water
μ_a	Viscosity of Air
μ_w	Viscosity of Water
α_a	The Volume Fraction of Air
u_p	The Velocity of Particle
u	The Velocity of Fluid Phase
ρ_p	The Density of Particle
F_a	Additional Force
Vs	Terminal Settling Velocity, cm/sec

Vi	Velocity of Particle i, m/s
Xi	Location of Particle i, m
Y	Young's Modulus, Pa
δn	Overlap Distance on Normal
δt	Tangential Direction
τ	Shear Stress, Pa
γ	Shear Rate, sec-1
Rei	Reynolds Number
Ef	Volume Fraction of The Fluid
Uf	Fluid Velocity in m/s.
Up	Cell Averaged Particle Velocity in m/s
Mi	Mass of Particle i, kg
CFD	Computational Fluid Dynamics
TFM	Two-Fluidmodel
VOF	Volume of Fluid
DPM	Discrete Phase Method
DDPM	Dense Discrete Particle Model
DEM	Discrete Element Method
DNS	Direct Numerical Simulation
LMC	Low Mach Code
FEM	Finite Element Method

1. INTRODUCTION

1.1. STATEMENT AND SIGNIFICANCE OF THE PROBLEM

Nowadays, understanding settling velocity and proppant transport in complex fracture system plays an essential role in determining propped fracture area, fracture conductivity, and their impact on well productivity and economics. Both experimental and numerical modeling are required to investigate proppant transport efficiency. Proppant transport is governed by several factors such as varying of settling velocity, fluid rheology characterization, fracture geometry, proppant size, and proppant concentration. In this study, computational fluid dynamics is carried out and used to model proppant transport through different complex fractures with various proppant size. The impact of the interaction between particle to particle and particle to fluid was captured using the domain fictitious method. To test and calibrate our simulation model, the study performed a validation simulation process against experimental observation of proppant transport.

In recent years, the oil industry has adopted the use of high viscosity friction reducers (HVFR's) in fracturing fluids due to several operational and economic reasons (Hu, et al. 2018; Van Domelen et al. 2017; Motiee et al. 2016; Ba Geri et al. 2019). HVFR fluids can replace slickwater by minimizing proppant pack damage and carry same amount of proppant as linear gel or better with less formation damage. (Ba Geri et al 2019b, Kunshin et al 2018). Hu et al. 2018 solved some problems which related to proppant transport capability using HVFRs and linear gel. In order to compare HVFRs with linear gel, viscosity and elasticity measurements were needed to investigate. Dahlgren et al. 2018 identified three field case studies in which STACK play replaced traditional fracturing fluid

with HVFR. Viscosity-shear measurements were made at 2, 3, and 4 gpt HVFRs concentration with and without a breaker. They noticed that the breaker had the negative influence for the viscosity profile. Ba Geri et al. 2019 conducted an experimental work to investigate the rheology and settling velocity in HVFR and linear gel under different conditions. They observed that HVFR had better proppant settling velocity performance compared to linear gel. Most of the work performed so far were either experimental work or field trail tests and not much work used numerical simulator to mimic the proppant settling performance in HVFR. Thus, this work was to build a numerical model using computational fluid dynamics (CFD) that can predict and provide better understanding of proppant transport in complex fracture systems using HVFR fracture fluids.

1.2. SCOPE OF THIS STUDY

Here is the scope of my work(Figure 2.1） including experimental work and simulation work. Each part will be illustrated.

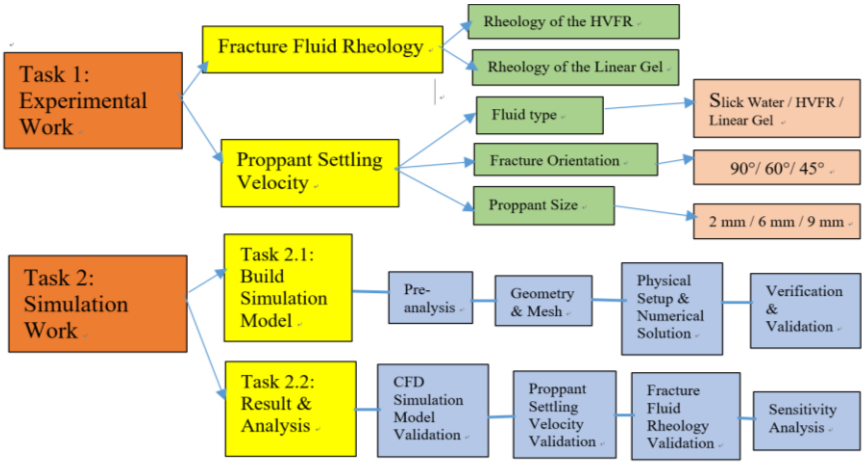

Figure 1.1. Scope of my work.

2. LITERATURE REVIEW

2.1. FRACTURE FLUIDS

Conventional fracturing fluids include water based and polymer containing fluids, hydrocarbon-based fluids, energized fluids and foam whereas unconventional fracturing fluids are categorized as viscoelastic surfactant fluids, methanol containing fluids, and liquefied petroleum gas-based fluids. In conventional fracturing fluids, slick water, linear gel and HVFR are discussed in detail with their composition, rheological properties, advantages, disadvantages and applicability.

2.1.1. Slick Water. Slick water is a method or system of hydro-fracturing which involves adding chemicals to water to increase the fluid flow. Fluid can be pumped down the well-bore as fast as 100 bbl/min. to fracture the shale. Without using slickwater the top speed of pumping is around 60 bbl/min (Wikimarcellus). Therefore, slickwater is a water-based fluid and proppant combination that has low-viscosity and it has been most widely used fracturing fluid especially in unconventional reservoirs.

The foremost components of this fracturing fluid are sand and water. Then other additives are mixed to solve different purposes like reducing the friction, corrosion, bacterial growth etc. Unlike the polymer solutions, viscosity of the slick water is very low because the only chemical which can substantially increase the viscosity is used in very low amount to reduce the friction while injecting the fluid downhole. Hence the amount of proppant which can be injected using slick water is very low (maximum 2.5 ppg) (Palisch et al., 2010) because of the less proppant carrying capacity and the fracture width created will be narrow as well from which very less amount of proppant can go inside the fracture.

Slick water has obvious advantages and disadvantages. The major benefits of using slick water as a fracturing fluid are reduced gel damage as very less concentration of polymer is used as a friction reducer, less cost, high stimulated reservoir volume and better fracture containment (Mohanty et al., 2012). The fracture length will be very long and reservoir-wellbore connectivity will be better because of the complex fracture network created by slick water (Gandossi, 2013). The lack of viscosity will also bring problems. Firstly, it needs high volume of water to inject sufficient. In addition, high pump rate is also required to overcome the friction losses and to ensure that sufficient amount of proppant reach to the tip of the fracture.

2.1.2. Linear Gel. Guar gum is often crosslinked with boron or chromium ions to make it more stable and heat-resistant. The crosslinking of guar with metal ions results in a gel that does not block the formation and helps efficiently in formation cleaning process. During a long period, guar is one of the most widely used polymer in the fracturing fluid which contains a long chain of polysaccharide with side chains of galactose and has high molecular weight (Jennings, A.R. 1996). Weaver and Schmelzl (2002) reported the average molecular weight of guar as 2-4 million Dalton approximately. It is usually used in the form of dry powder that swells when mixed with an aqueous solution and form a viscous gel (Gandossi, 2013). The viscosity attained using these linear polymers is around 35-50 cp (Al-Muntasheri, 2014). This viscosity is sufficient enough to carry at least much more amount of proppant than any usual slick water will carry.

The oil company developed derivatives of guar such as hydroxypropyl guar (HPG) and carboxymethylhrdroxypropyl guar (CMHPG) whereas the other forms of cellulose based polymers are carboxymethyl cellulose (CMC), hydroxyethyl cellulose (HEC) and

carboxymethylhydroxyethyl cellulose (CMHEC). Among them HPG and CMHPG are the most common gelling agents used for fracturing.

The linear gels with that high viscous prevent fluid loss by creating a filter cake on face of the low permeability formation but damages the formation conductivity by leaving the polymer residue at the same time. In high permeability formation the behaviour of linear gel be completely opposite and the amount of fluid loss will be high as there would not be any mud cake created on the face of the formation (Gondassi, 2013). Guar concentration to prepare linear gel on the field is reported to be 0.12-0.96 w/w for operations (Robert and Pin, 1993). As long as clean up property of guar is concern, the expected residue is approximately 6-10% by weight and is less for HPG which is around 2-4% by weight. (Economide et al., 2000)

2.1.3. High Viscosity Friction Reducers (HVFRs). As we discussed before, friction reducers (FRs) are used to decrease the amount of power required to move a hydraulic fracturing fluid through a formation at a fixed flow rate. Though FR viscosity is not a crucial consideration in proppant transport when used before the perforations in slick water applications, FR viscosity becomes a greater consideration in proppant transport from the perforations into the formation and an important qualifying criterion with the advent of High Viscosity Friction Reducer (HVFR) systems that require higher loadings than traditional FRs. Consistent viscosity measurement can vary greatly depending upon a number of factors, for example temperature, hydration approach, polymer concentration, brine composition, and additive interaction. A study was developed and implemented to determine the influence of HVFR by concentrated particulate and bead settling. Y. Thomas Hu (2018) compared the proppant transport capability of apolyacrylamide-based HVFR

with that of linear guar at cost-parity concentrations and the results indicate that the proppant transport performance of fracturing fluids correlates better with their elasticity and low shear viscosity than the high shear viscosity. Kyle Dahlgren and Brett Green (2018) indicated three case studies of high viscosity friction reducers HVFR in the STACK Play and they finally found that high viscosity friction reducers as a successful fracturing fluid in the STACK play and require further testing and development in the field.

Matt Johnson (2018) used HVFR in marcellus shale stimulation and the benefit of HVFRs is founded. Many HVFRs are available as a single fluid system that can be adjusted to provide a range of viscosities, which makes the operation at the wellsite much simpler to execute. Not only does it lower the number of chemicals required onsite, it also reduces tank requirements and the number of trucks in the field. In addition, its and handling equipment are not required due to the relatively rapid hydration rate for HVFR polymers (Van Domelen et al. 2017). The friction reducing properties of the HVFR fluid allow it to be pumped downhole at lower hydraulic horsepower requirements. What's more, the ability of HVFRs to increase fluid viscosity at relatively low concentrations means that more proppant can be transported with less water in the formulation, which is a significant cost reduction benefit for operators who are constantly looking for ways to lower their operating expenses.

2.2. RHEOLOGY OF THE HVFR AND THE LINEAR GEL

High viscosity friction reducers (HVFRs) plays an important role in reducing the cost and improving retained conductivity. It means, comparing to the traditional linear gel, HVFRs is more popular and more competitive (Y. Thomas Hu, David Fisher, 2017). But

HVFRs has its own shortcomings. HVFRs may not be as good at transporting proppant as traditional linear gel, but this assumption also requires further scientific experiments to confirm. HVFRs can replace the mixed fracturing fluid in unconventional reservoir completions, and it is one of the important components of viscous slick water. We need to better understand the nature of HVFRs so that we can make better use of it. Therefore, the rheological properties of HVFRs are very important, especially viscosity.

There are many hydraulic fracturing treatments use gelled fluids because of their high viscosity which can create wide enough fractures that can take sufficient amount of proppant inside it. The fracture will start closing when the pumping process is stopped and conductive channels will be created due to improper closure of the fractures caused by the proppants settled in between those fractures. Harris and Morgan, 2005 found that the rheological properties of the fluid such as apparent viscosity, yield stress, viscoelasticity, dynamic viscosity, etc, directly affect the properties of the fracturing fluid, thereby affecting the load carrying capacity of the proppant. Sharma, 2012 and Gomma et al., 2015 found that consideration of viscosity alone could not accurately assess proppant transport and hence effects of elasticity on the proppant transport need to be investigated.

2.2.1. Viscosity of the HVFR. Viscosity is the material property which relates the viscous stresses in a material to the rate of change of a deformation. On the other words, viscosity is a measure of the fluid’s resistance to flow. In general way, steady shear sweep test is performed to identify the fluid’s viscous characteristics in which shear stress is measured for each shear rate implemented.

The standard measure of fluid flow resistance is viscosity. In the field of human research, Newtonian fluids and non-Newtonian fluids represent essentially all fluids.

Another important physical parameter is the shear rate. The viscosity of most fluids, represented by HVFR, depends on the rate of shear rate, but the viscosity of Newtonian fluids is always constant. Shen (2018) use advanced rotational rheometer to do this experiment. Both high shear and low shear viscosity was measured at HVFR concentrations of 2, 4, 6 and 8 gpt (gallons per thousand gallons).

Carl Aften, Solvay S. A（2018）illustrates a characteristic rheological curve shown in Figure 2.2 for a shear thinning water-soluble polymer, with Stokes' law of settling principle accepted, and a high viscosity Newtonian plateau present at low shear rates. The majority of the fluid's s shear profile resides at the higher shear rate end of the rheogram demonstrating the actual flow from the pumps to the perforations and represented by a presumed low viscosity Newtonian plateau.

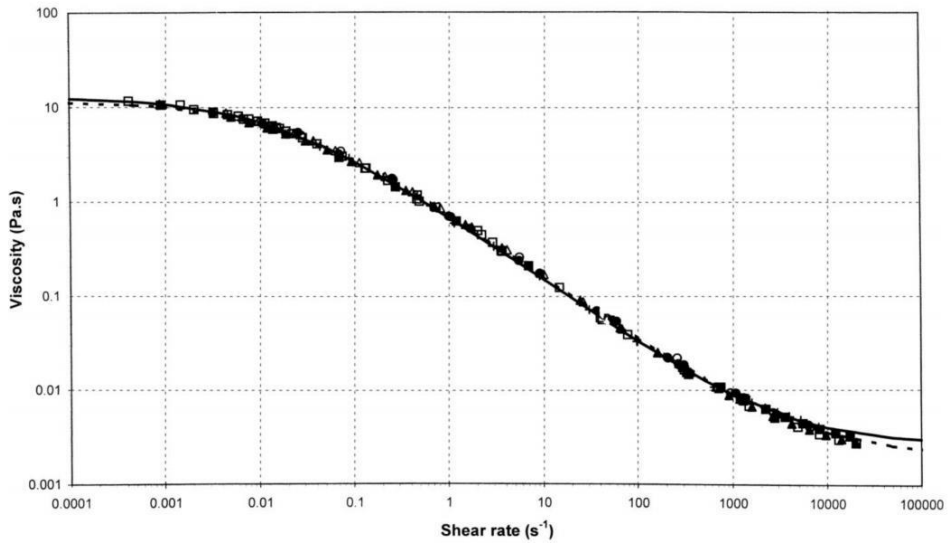

Figure 2.2. Ideal rheological profile of a water-soluble polymer (Escudier, 2001).

Three scientifically researched and documented principles of proppant transport that characterize the balance and effects of velocity and viscosity interrelation, listed in order of decreasing velocity and increasing viscosity influence are Newton's, Allen’ s, and Stokes’ laws.

Thomas Hu, etc. (2018) showed field data where HVFRs were used in the place of linear gels to deliver proppants and they generate "plug-and play" HVFR formulations that can directly substitute linear guar at a given concentration. The rheological test results show as the Figure 2.3 below, at each comparative concentration (i.e. 2.25 gpt HVFR versus 15#guar; 3 gpt HVFR versus 20# guar; 4.5 gpt HVFR versus 30# guar), the HVFR had a lower viscosity at intermediate to high shear rates but higher viscosity at low shear rates. The shear rate at which the HVFR and guar had the same viscosity was 16 for 2.25 gpt HVFR and 15# guar, and decreased to single digits for the other two pairs of fluids. In addition, the slot flow clearly shows that the HVFR had better sand carrying capability than guar. One reason for the improved proppant transport could be the larger viscosity of the HVFR at low shear rates. Even though the average shear rate in the slot is about 80, the shear rate is much lower in the vicinity of the slot center due to the non-uniform nature of the Poiseulle flow. Therefore, in this region particles will be suspended in the HVFR for a longer time than in guar and travel much longer before they settle to the bottom. Three cases shown in Kyle Dahlgren and Brett Green’s (2018) research. The first includes two nearly identical offset horizontal wells in terms of landing target, location, and completion designs. The lone differing variable between the two wells was a substitution of HVFR for gel, both linear and crosslink, in the pump design. The second case describes an application in an extended-reach lateral within thinning pay to optimize economics in stressed areas.

The last case includes a horizontal lateral in the geologic heart of the play with consistent well results in surrounding sections.

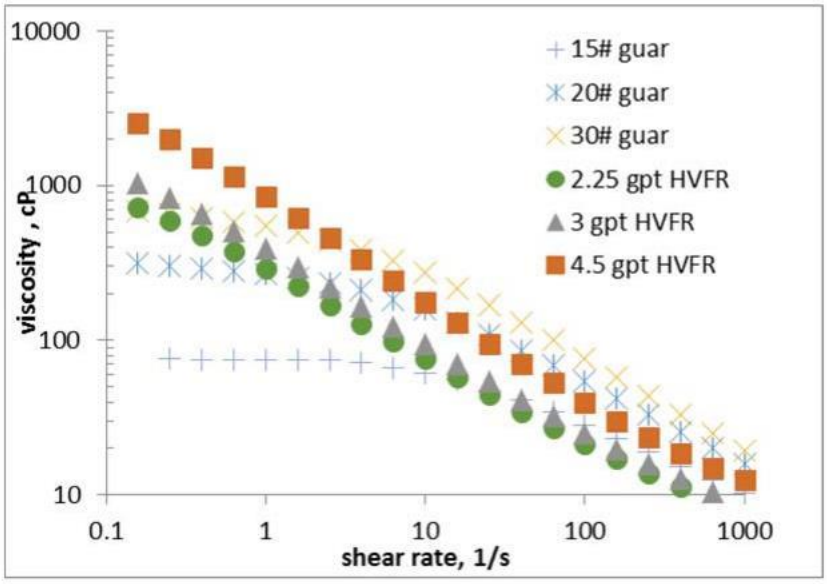

Figure 2.3. Viscosity as a function of shear rate for the HVFR- and guar-viscosified fluids (Thomas Hu, etc. 2018).

The fluid rheology testing showed that the breaker provides a distinct reduction in the viscosity of the HVFR as compared to the fluid system without the breaker and friction reduction has been evaluated with the HVFR in a laboratory flow loop and consistently provides friction reduction values of around 70%, regardless of variations in the mix water composition.

StimLube HBVB which indicated by Matt Johnson (2018) was thoroughly evaluated in laboratory studies designed to measure the product's ability to build viscosity under a wide range of treatment dosages and water hardness levels. StimLube HBVB was evaluated in these viscosity tests at the common loading rates ranging from 1to 5 gpt.

2.2.2. Viscosity of the Linear Gel. Two major types of fluids have been discussed previously: Newtonian fluids and non-Newtonian fluids. However, in the case where the subject is a non-Newtonian fluid, the viscosity is in fact constantly changing according to different shear rates, and there is no constant value. Non-Newtonian fluids are further divided in sub-classes such as shear thinning or pseudoplastic fluids, shear thickening, viscoelastic etc. Chhabra (2007) illustrated the detailed description of all the different classes of non-Newtonian fluids. Most linear gels or uncrosslinked gels are considered to be non-Newtonian shear thinning because their viscosity decreases as the shear rate increases. In reality, however, most polymer fluids exhibit shear thinning behavior. Under long-term research observations, it was concluded that the rate of decrease in viscosity with shear rate depends on factors such as the type and concentration of the polymer used, the molecular weight of the polymer, the type of solvent, and the temperature. As linear gel is shear thinning non-Newtonian fluid, value of effective viscosity is used for calculations which is taken at values of apparent shear rate (particle shear rate caused by the movement of the sphere falling in a quiescent fluid) between Vs/dp and 3Vs/dp (Roodhart, 1985). From the Table 2.1 below, it contains the information regarding the different linear gels used by previous researchers according to the concentration of the polymers used to prepare the linear gel (‘n’ determines the degree of shear thinning).

Table 2.1. Viscous characteristic of various fracturing fluids.

Author	Fluids	Density (gm/cc)	n	Range of shear rate (sec-1)
Clark et al. 1981	HPG	NA	0.829-0.293	0-150

Table 2.1. Viscous characteristic of various fracturing fluids (cont.).

Roodhart 1985	Guar gum / HEC	NA	0.33-8.5 / 1.4-40	0.1-1000
Kirkby and Rockefeller 1985	HPG	NA	NA	0.01-1000
McMechan and Shah 1991	HPG / HEC	NA	NA	NA
Machac and Lecjaks 1995	Tylose / Natrosol / Kerafloc	1.00	0.898 / 0.741 / 0.356	1.5-16.2
Asadi et al. 1999	Guar gel / HPG	NA	NA	600
Goel et al. 2002	Guar gel	NA	NA	0.1-1000
Kelessidis and Mpandelis 2004	CMC	1.00 (20 ℃)	0.7449-0.9099	5-1000
Liu and Sharma 2005	Guar gel	NA	0.59	5-1022
Hu et al. 2015	CMHPG	NA	0.62	10-100
Shahi and Kuru 2016	CMC	NA	0.8	0.1-1000
Arniaplly and Kuru 2017	HPAM	NA	0.35	1-200

2.3. MEASUREMENT OF SETTLING VELOCITY IN CONFINED FLUID

In recent decades, researchers have used different methods to study the settlement problems in closed fluids. Lecjaks (1995) used six different sizes of spheres and glycerol of different densities as Newtonian fluids, Tylose, Natrosol and Kerafloc as non-Newtonian viscoelastic fluids, using rectangular columns of 80 cm height, 8 cm longer width and 1.2

cm shower width. Based on its experimental results, it has a wide range of applicability and is equally applicable to square pipes. Sharma (2005) used 40 pptg linear guar, water and a mixture of water and glycerol in the experiment to study the effect of fracture wall on the settling velocity of proppants under static conditions. By analyzing the results obtained from the parallel plate model using proppants of different sizes and specific gravities, they found that as the viscosity of the fluid increases, the fracture wall effect becomes more pronounced and the settling velocity is gradually decreasing. This effect represents a change in the rate of settling. As the ratio of particle size to fracture width increases, the settling velocity of both Newtonian and non-Newtonian fluids decreases. They observed that increasing the shear thinning of the fluid reduced the wall delay effect.

What's more, Malhotra（2012）got something new. It is observed in his experimental results that increasing the shear thinning behavior of the fluid reduces the wall delay effect. Even the elasticity of the fluid delays the influence of the wall, and as the ratio of the particle size to the fracture width increases, this delay becomes more significant.

Previous authors also doing research about the effect of size of the proppant and viscosity of the fluid on the settling velocity of the single proppant with confining fracture walls. Liu and Sharma (2005) found that with increasing viscosity of the fluid, effect of fracture walls increase in their experiment using ceramic proppants. After their data analysis, the decrement in the settling velocity inside water is 24% when the fracture width narrows down from 5.5 cm to 0.27 cm whereas in the case of 10 pptg gel the reduction increases to 31% and for 20 pptg the reduction increases more to 45%. Therefore, from the values of decrement percentage, it can be concluded that increasing viscosity of the fluid

increases the hydrodynamic interaction between proppant and fracture walls due to which the reduction in the settling velocity increases. This phenomenon was not observed in all the cases may be due to usage of actual proppants in which the size and the specific gravity of the proppant can never be exactly same for every single particle used during experiments.

2.4. STATIC SETTLING VELOCITY SIMULATION

Literature review of static settling velocity simulation is required before starting a new research about simulation. Different simulation model brings different numerical methods to solve the problem. Table 2.2 includes name, year, experiment, simulation approach, proppant size and fluid type of previous authors. Learning about what others do helps me choose my own model to setup the simulation work.

Table 2.2. Different simulation model used by several authors and the details.

Author	Year	Experiment	Simulation Approach	Proppant Size	Fluid Type
Phani B. Gadde, Yajun Liu et.al	2004	NA	UTFRAC-3D	NA	Slick Water
G.Pianet, E.Arquis	2007	Yes	DNS	DP=6.25	Water
Jan Erik OLSEN and Schalk CLOETE	2009	NA	VOF/DPM	NA	Gas
Jenny Suckale	2012	NA	CFD	NA	Water

Table 2.2. Different simulation model used by several authors and the details (cont.).

Christoph Kloss and Christoph Goniva	2012	NA	CFD-DEM	5mm	Water
Xizhong Chen and Junwu Wang and James McAndrew	2014	NA	CFD-DEM/CFM/DDPM	0.65mm	Water
Pratanu Roy. Wyatt L .Du Frane et.al	2016	Yes	LLNL SAMRAI	D=500	Water/Oil
Rongqian Chen, Yi Liu et al.	2017	NA	LB-DF/FD DNS	NA	Non-Newtonian fluid
Songyang Tong, Robin Singh and Kishore K	2017	Yes	CFD	20/40 ceramic proppant	Water
Xianhui Kong and James McAndrew	2017	NA	CFD-Euler-Euler multiphase	200um/400um/600um /800um	Water
R.Kou, G. J.Moridis et.al	2018	Yes	CFD-DEM	50/70	Water/ Oil

Particle sedimentation is one of the most common phenomena in nature and industrial production, such as fluidized bed, gas filtration technology and sand deposition, which always presents classic problems in the field of fluid dynamics. The application in petroleum engineering is also very extensive. For example, we have studied the

sedimentation of particles in different viscosity fluids to provide a more comprehensive understanding of the proppant migration in the downhole fracture. The difficulty in studying the sinking of particles in still water is the interaction between the particles and the possible wall-effect of the particles and the wellbore.

Jan Erik OLSEN and Schalk CLOETE (2009) talks about the volume of fluid (VOF) model and the discrete phase method (DPM) in their article, which is highly used in my research later on. They focus on the coupled DPM and VOF model which is applied to gas stirred ladles with bottom injection and validated against experiments. It is shown that the assumption of a flat surface is acceptable if the purpose is to obtain velocity profiles at different elevations in the ladle. If mixing time is the purpose of the investigation, the flat surface assumptions is not valid. The model is also applied to prove that the lift force is not significant at higher gas rates.

They choose to study the hydrodynamics of a ladle, which means the liquid is in the ladle and the gas above the liquid and the bubbles in the liquid. In some case, the ladle may contain secondary liquid phases or the top gas may be ignored and cause a boundary condition problem. Sometimes the boundary condition problem is the hardest to deal with. The coupled Volume of Fluid (VOF) and Discrete Phase Model (DPM) applies the VOF model to describe the fluid behaviour of the liquid in a ladle, the continuous gas phase above the liquid and the interface between them. Since the VOF model cannot resolve the bubbles with an affordable grid resolution, a Lagrangian method, DPM, is used to track the bubbles, which is the biggest advantages of Discrete Phase Model.

Actually, they do not have the experiment result to compare with. So, they use their modeling results compared to experimental results (Engebretsen et.al., 1997) to validate

the model. A series of experiments were conducted in a rectangular basin with a depth of 6.9 m and a surface area of 6 x 9 m. The basin was filled with water and air was released at the bottom at gas rates of 83, 170 and 750 Nl/s (equivalent to 50, 100 and 450 l/s referred to the state at the inlet). The inlet was comprised of a release valve with a rapidly acting piston injecting gas vertically with arrangements in front of it to reduce the vertical momentum. Because of this momentum breaker, the fluctuations in the gas flow and the length of the inlet jet were minimized. They also see from Table 2.3 that the time it takes for the first bubbles to reach the surface is well predicted by the model which is the most important in the modeling.

Table 2.3. Experimental and theoretical bubble rise times (Jan Erik OLSEN 2009).

Gas Rate	83 Nl/s	170 Nl/s	750 Nl/s
Experimental	6.0 s	4.8 s	3.1 s
Modelled	6.6 s	5.2 s	3.1 s

In their research, the method is a coupled VOF and DPM model which is numerically robust and efficient. By applying the method to gas stirred ladles with bottom injection, it has been shown that the lift force has no influence on the hydrodynamics for higher gas rates. Besides, it has also been shown that the assumption of a flat surface is acceptable if the purpose is to obtain velocity profiles at different elevations in the ladle.

Xizhong Chen and Junwu Wang（2014）mentioned the Eulerian-Eulerian two-fluid model (TFM) and the discrete element method (DEM) in their article. The Eulerian-Eulerian two-fluid model (TFM) treats both gas and solid phase as interpenetrating

continua, the conservation equations of mass, momentum and energy are obtained through an appropriate averaging process and the constitutive relations for solid phase are usually closed using kinetic theory of granular flow (J. Ding. 1990). The TFM method normally requires much less computational resources compared to Eulerian-Lagrangian approaches. Therefore, it can be used to model and study pilot scale and industrial scale reactors (X.-Z. Chen. 2011). Despite the advantages, the discrete character of the solid phase is lost in the TFM method owing to the continuum description of the dispersed phase. This limitation can be overcome by discrete approaches such as discrete element method (DEM) (Y. Tsuji.1993), in which solid particles are tracked individually according to Newton's laws of motion with detailed particle-particle and particle-wall collisions. One of the main drawbacks of DEM method is the high computational demands (M. Xu. 2012), which restricts its applications to small scale, fundamental investigations.

In the TFM, the particle-particle and particle-wall friction is not considered; therefore, in the CFD-DEM simulation, only the normal particle-particle and the normal particle-wall collisions were included to maintain consistency with KTGF. About the DEM method, the advantage of the DEM approach over the other two models lies in its explicit treatment of the particle-particle collisions. The interactions between two particles are represented as spring and dashpot in DEM method, where the spring causes the rebound off the particles and the dashpot mimics the dissipation of the kinetic energy due to inelastic effect.

The TFM method and DPM method have more potential for industrial applications since they are less computational demanding. However, the limitations of these methods should be known. TFM method always predicted a converging flow and failed to predict

the particle trajectory crossing effect in dilute system, while the DPM method failed to predict the cases where the two particle jets are emerging. At the same time, both TFM and DPM successfully reproduced the main features of impinging flow at some cases.

Pratanu Roy (2016) and his research team get a incredible research on numerical and experimental studying of particle settling in real fracture geometries. When I read Roy's paper, I was deeply shocked by the ability of their team to analysis data with such high quality.

Based on their real fracture experiment result, the perspective of modeling proppant transport has a pretty big challenge because the experiment combines multi-component fluid behavior with thin-film or lubrication flow. The thin-film always cause the wall-effect and the lubrication flow will increase the pressure of calculating the modeling result in the last simulation part. They investigate the transport properties of particles in fractures through a series of high-fidelity numerical simulations and sub-fracture-scale experiments. After the experiment work, they got the proppant movement in clear-plastic three-dimensional reproductions of the shale surfaces recreated using three-dimensional printing. In addition, they use tailored flow cells to combine with microcapsules for improved particle tracking in dense particle packs. About the real fracture environment, the flow cell consists of two pieces: the “roof” and the “floor” shown on Figure 2.4. The “roof” of the cell containing one half of the fracture surface and the “floor” containing the opposite surface along with the entry and exit part.

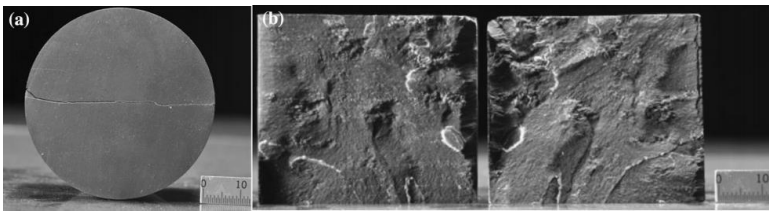

Figure 2.4. Marcellus shale sample a top view of core, the original sealed fracture and induced fracture path are evident running across the center of the core; b fracture surfaces (Roy. 2016).

Later on, they made a synthetic proppant analogue consisted of a mixture of transparent microcapsules shown on Figure 2.5 to improve particle tracking during the experiment. The last part in his research is building the numerical model, then compare the simulation result with the experiment result. The simulation uses the LMC-SAMRAI code which based on a distributed Lagrange multiplier technique in which both the interstitial fluid and particles are fully resolved and coupled (Patankar et al. 2000; Glowinski et al. 1999), for direct numerical simulation of particulate flow (Kanarska et al.2011).

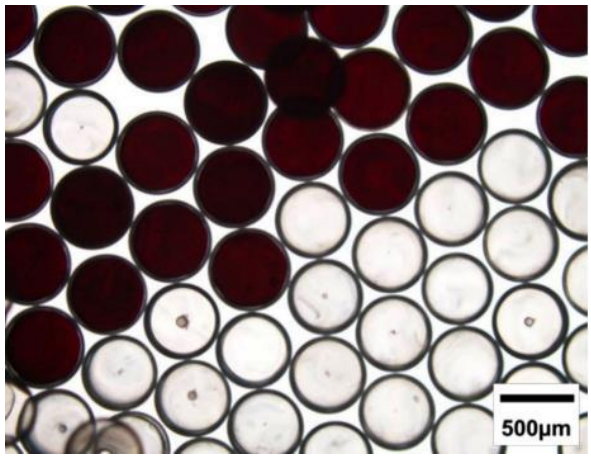

Figure 2.5 . Examples of hydro-dynamically identical transparent-bulk and Opaque-tracer particles created using micro-encapsulation (Roy. 2016).

They got the net result which was the rapid formation of regions of high particle concentrations interspersed with clear regions virtually devoid of proppant particles in Figure 2.6. Figure 2.6(b) give the evidence of the upwelling fluid which is sufficiently strong that particles become entrained in this upward fluid flow. This figure illustrates the probability density distribution of the settling speeds of the individual particles. While the net motion for the bulk of the particles is downward, a small percentage of the particles have a positive vertical velocity. In Figure 2.6 (a) we can see some particle paths with vertical velocity components which reveals that the upward components are generally aligned with the regions of the fracture with relatively low particle concentrations.

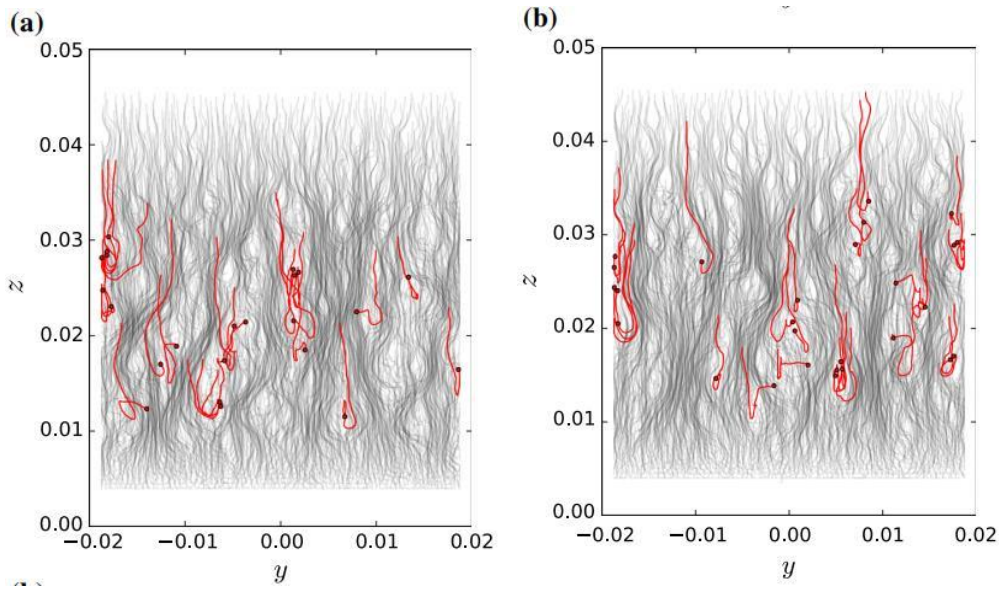

Figure 2.6. Particle paths during settling in the fractured sample and between two parallel plates. The red lines indicate the paths of some particles that reverse in direction with markers (not to scale) indicating the particle locations at the final timestep. Axes given in meters (color figure online) (Roy. 2016).

They finally found that new experimental and numerical methods capable of resolving sub-fracture scale behavior are needed to better understand the behavior of proppant in fractures and improve these empirical models because these models may underestimate the effect of the fracture geometry on the proppant behavior. I found this problem in my case, too. I finally realize that I need to combine the air effect and the wall effect in my CFD-FLUENT model.

Rongqian Chen (2017) found that a direct numerical simulation (DNS) is usually adopted to study the mechanism of particle sedimentation. In a DNS method, the fluid flow and particle motion are coupled to study the dynamics of individual particles suspended in fluids, which is the highest resolution numerical method without any empirical model. In addition, his work focuses on the boundary condition and the curve boundary of particles. Dealing with the curve boundary of particles in the simulation via the DNS method is pretty important. In the past research, there are two kinds of schemes which are usually adopted to simulate the particulate flows: the immersed boundary method (C. S. Peskin. 1977) and the fictitious domain method (R. Glowinski. 1999). Chen's group want to know under what circumstances the particles are falling together in the channel. Therefore, they use lattice Boltzmann direct-forcing/fictitious domain (LB-DF/FD) method to simulate the sedimentation of three circular particles in a vertical channel. Figure 2.7 shows the schematic of the problem.

After doing the experiment, they analysis the experiment data and made a validation. The sedimentation of a circular particle in a narrow channel is adopted to validate the present computation method.

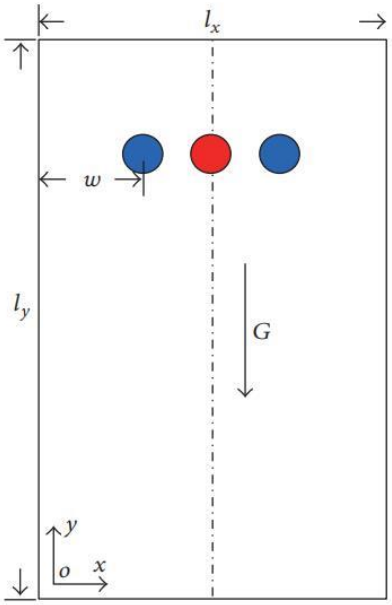

Figure 2.7. Schematic of the problem (Rongqian Chen. 2017).

It can be inferred that the particle moves away from the wall and undergoes a damping oscillation about the centerline of the channel until it reaches a steady state. They finally completed the LB-DF / FD method to simulate the settlement of three particles in a narrow channel. The effects of wall and Reynolds number on particle trajectories are also studied. Results have shown that at certain Reynolds numbers (Re= 10 or 40 < Re $\leqslant$ 100) the left particle always sediments at 0.175 of the channel widths irrespective of its initial position or the channel width. In addition, results have also shown that the lateral particles lead at small Reynolds numbers, while the central particle leads at large Reynolds numbers. Therefore, doing research about Reynolds numbers is necessary.

R. Kou and G. J. Moridis (2018), they focus on providing a better understanding of proppant transport behavior in inclined planar fractures by means of numerical simulation. They found a significant difference from prior (laboratory) experiments is the capability of

their model to simulate proppant transport at field-scale flowrates. Such capability is critical in understanding proppant transport and appropriately designing it by ensuring that the correct Reynolds number and flow regime are used in the design calculations.

Although I am studying the settling velocity in the static water, but I can also learn a lot from the dynamic proppant transport, which is popular in recent petroleum industry. Because the understanding of proppant transport in fractures plays a critical role in estimating propped fracture dimensions and performance. Modeling of such processes is challenging because of the complex interactions between fluid, proppant particles and fracture geometry. So, Kou and G. J. Moridis found that existing models generally assume vertical planar fracture geometry, whereas the reality in the subsurface maybe much more complex. Therefore, they use discrete element method and computational fluid dynamics simulations in this study which I mentioned before to demonstrate that interactions between proppant particles and fracture side walls play an important role in proppant transport efficiency.

They use two validation ways that they thought would be better to describe particle settling tests and laboratory proppant transport experiments. They use two hydraulic fracture simulation at the beginning, one with a vertical planar fracture (as a base case), and the other with an inclined planar hydraulic fracture. They conducted proppant transport simulations using our benchmarked models in both domains and compared the proppant distribution results. Different from Jan Erik OLSEN and Schalk CLOETE (2009) who use the volume of fluid (VOF) model and the discrete phase method (DPM) for simulation, Moridis's group choose DEM simulation using LIGGGHTS (Kloss et al. 2012), which is an open source C++ simulator built on the LAMMPS (Plimpton,1995) platform and

parallelized with MPI and CUDA. Actually, using DEM is much more complex than using CFD-FLUENT because it needs reliable computer code to work with.

In the next part, Moridis's verification method has benefited me a lot. And I innovatively used a graph of time related to particle drop distance to validate my model. In their part, they conducted a simulation that described a laboratory test of a settling proppant particle and the simulation study involved tracking a spherical particle with a diameter of 0.512 mm (representing 50/70 mesh sand) that is dropped in a water container. The evolution of the velocity of the descending (settling) particle is shown in Figure 2.8. The particle initially accelerated under the influence of the gravity force, and eventually it reached terminal velocity. Because of the limitation of Stokes equation, they conducted laboratory settling tests using 3 different-sized particles (20/30 mesh, 30/40 mesh and 50/70 mesh) and two types of fluids (water and oil) to calibrate their model over the full range of Reynolds Number which can match the simulation result much easier.

The results show that the terminal velocity estimated from the coupled CFD-DEM simulation matches well the experimental data, but the agreement with the analytical solution deteriorates as the particle size increases. For slick water hydraulic fracturing operations, they indicate that near wellbore proppants consist of both early- and late-stage injected proppants, besides that, their model tend to indicate that proppants near the wellbore are those last injected which is different from the previous models which other people does. After learning his research, we finally give up using CFD-DEM as our basic model. The reason is simple. CFD-FLUENT can get better result for complex boundary condition situation and is much easier to use.

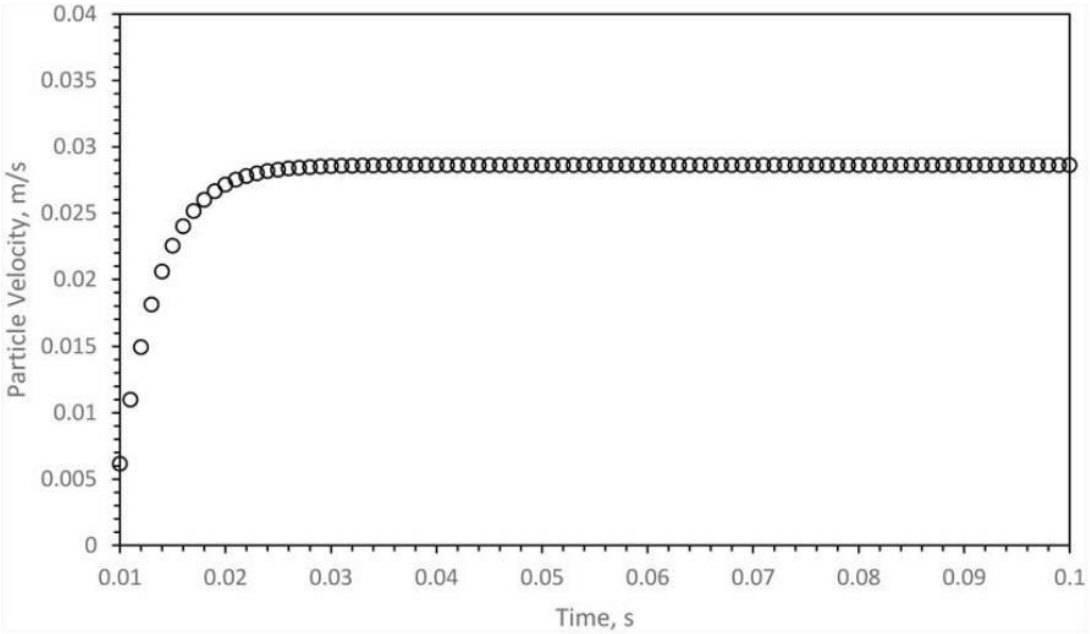

Figure 2.8. 50-70 mesh sand settling velocity in water (Moridis. 2018).

3. PROPPANT SETTLING EXPERIMENTAL DESCRIPTION

3.1. EXPERIMENT MATERIALS

Three fracturing fluids were tested including slickwater, HVFR, and linear gel. HVFR and linear gel samples were obtained from BJ Services. HVFR was prepared according to the standard industry practice of using HVFR, where 2 gpt concentration of HVFR were mixed with deionized (DI) water. Different sizes (2 mm, 4 mm, and 6 mm) (Figure 3.1) of glass beads proppant were used to measure proppant terminal settling velocity. High accuracy advanced rheometer with a parallel-plate system was used to measure fracture fluid viscosity-shear profile at lab temperature conditions. The particles were painted shown in the Figure 3.2 so they can be more visible in the vague fracture fluid.

Figure 3.1. Different sizes (2 mm, 4 mm, and 6 mm) of glass beads proppant.

Figure 3.2. Painting particles.

3.2. CONFINED FRACTURE WALL EXPERIMENT SETUP

Figure 3.3 shows the schematic of the experimental fracture cells setup. The fracture cell model dimensions were 50 cm height and 7 cm length and kept the same for all the experiments. Fracture cells were constructed of two Plexiglas plates that were perfectly fit parallel and smoothly. Gasket rubber was placed between the parallel plates which mimics the fracture width. Two different fracture widths were studied: 3 mm and 9 mm. At this point, the cell was filled by either slick water or HVFR fluid and positioned the cell vertically. High-resolution video camera used to record the proppant settling process. Proppant sizes of 2 mm, 4 mm, and 6 mm were used to conduct experiments. Figure 3.4 shows the experiment picture in laboratory.

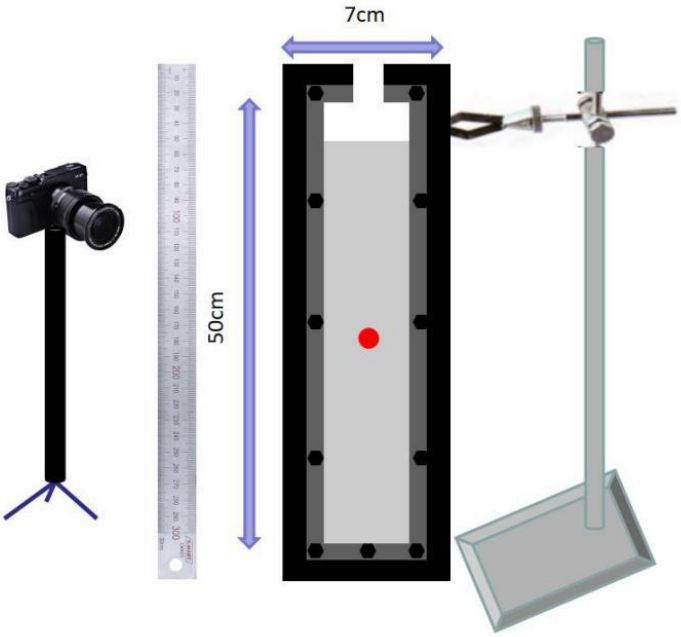

Figure 3.3. Schematic of fracture setup for confined fluids.

Figure 3.4. Realistic model in lab.

In complex fracture system includes numerous of natural fracture which inclined from the main fracture by variety of angles. Understanding proppant settling behavior in inclined fracture is an essential for proppant transport in fracture treatment. Three different angles 45º, 60º, 90º have been investigated to mimic inclination fractures. The configuration of this experiment for modeling the particle-wall friction occurred due to the interaction between particles and inclined walls effect. Confined fracture wall setup was positioned as illustrated in Figure 3.5 to observe the fracture inclination effect. Spherical proppant shapes used with diameter ranges of 2 mm, 4 mm, and 6 mm. The motion of proppant rolling down in the inclined cells acting under four forces friction force Ff, gravitational force, FG, buoyancy force FB, drag force, FD, and Fr, friction force.

$$F_f = mg \sin\theta \tag{1}$$

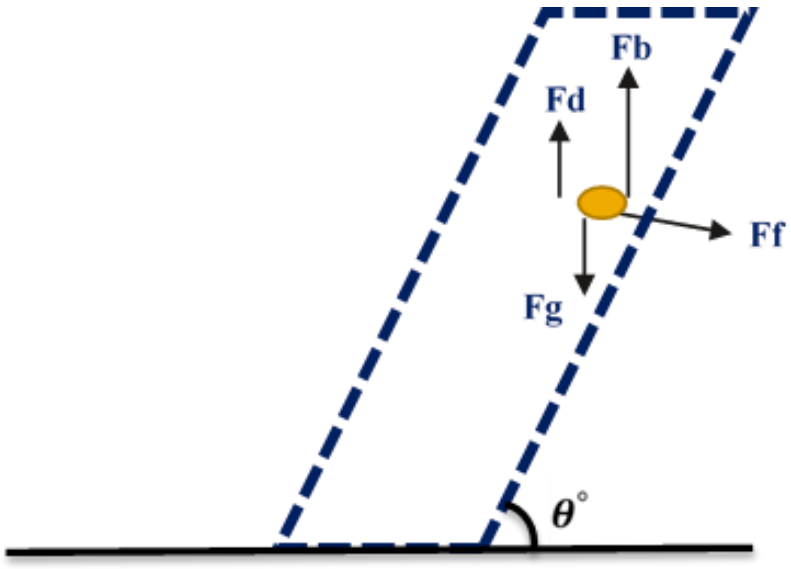

Figure 3.5. Schematic of the experimental fracture cell for measuring inclination angle effect.

Figure 3.6. Angle effect experiment process record in lab.

4. COMPUTATIONAL FLUID DYNAMICS (CFD) BASICS INTRODUCTION

4.1. WHAT IS CFD?

ANSYS, Inc. is an engineering simulation software (computer-aided engineering, or CAE) developer headquartered south of Pittsburgh in the South pointe business park in Cecil Township, Pennsylvania, United States. One of its most significant products is ANSYS CFD, a proprietary computational fluid dynamics (CFD) program (Wikipedia).

Computational Fluid Dynamics (CFD) is a set of numerical methods applied to obtain approximate solutions of problems of fluid dynamics and heat transfer. Therefore, CFD is not a science by itself, it is a way to apply the methods of one discipline (numerical analysis) to another (fluid flow/mass transfer and heat transfer).

4.2. WHY CFD?

CFD is used because there are many engineering problems that can't be solved by analytical or Experimental approach, or it is difficult to use analytical or experimental approach. The reason is the analytical solutions are only possible for a limited number of problems, usually formulated in an artificial, idealized way and the experimental approaches are more suitable reliable real-world situations but sometimes the disadvantage is very obvious that the real-world situation is too expansive, besides, too many technical difficulties. In conclusion, CFD gives an insight to the pattern of the fluid flow that is difficult to predict with regular experiments, expensive to conduct and sometimes impossible to study by the regular experiments.

4.3. HOW DOES CFD MAKE PREDICTIONS?

The CFD software use mathematical tools to solve the problem which is a pre-set of equations. The main factor of CFD is:

- The researcher who feeds the problem into the computer.
- Scientific knowledge that is expressed mathematically.
- The computer code that consists of the algorithms that embodies the knowledge.
- Hardware of the computer that performs the calculations.
- The researcher who simulates and interprets the data.

CFD is a highly disciplinary subject that indulges into the research area and lies at the interface of physics, applied math and computer science.

4.4. APPLICATION OF CFD

CFD is a very powerful technique and spans a wide a wide range of industrial and non-industrial applications. Some examples are as follows:

- Aerodynamics of aircrafts and vehicles: Drag & Lift.
- Power plant: Combustion in internal combustion engines & Gas turbines.
- Hydrodynamics of ships.
- Biomedical engineering: Blood flow through arteries and veins.
- Environmental engineering: distribution of pollutants.

4.5. CODING IN CFD

CFD is solving basic equations of fluid flow and heat transfer by applying Numerical techniques. I wrote my own C language to solve my case which is static settling velocity simulation. My code in C language is:

```
#include "udf.h"
#include "dpm.h"

/*update the user scalar variables*/

DEFINE_DPM_SCALAR_UPDATE(track_particle,cell,thread,initialize,p)
{
        float time = RP_Get_Real("flow-time");
        float x = p->state.pos[0];
        float y = p->state.pos[1];
        float u = p->state.V[0];
        float v = p->state.V[1];
        float z = p->state.pos[2];
        float w = p->state.V[2];

        FILE *fd;

        fd = fopen("oneparticle.out","a");

        fprintf(fd, "%8.6e %8.6e %8.6e\n",time, x, y);
        fprintf(fd, "%8.6e %8.6e %8.6e\n",z, u, v);
        fprintf(fd, "%8.6e\n",w);

        fclose(fd);
}
```

4.6. ANSY FLUENT

ANSYS FLUENT is one of the most popular commercial CFD software packages. ANSYS FLUENT CFD Solver is based on the Finite Volume method that the domain is discretized into a finite number of control volumes in Figure 4.1 and general conservation equations for mass, momentum, energy, species are solved on this set of control volumes. I use ANSYS FLUENT in my case to make simulation of static settling velocity simulation with 2 mm (diameter) particle.

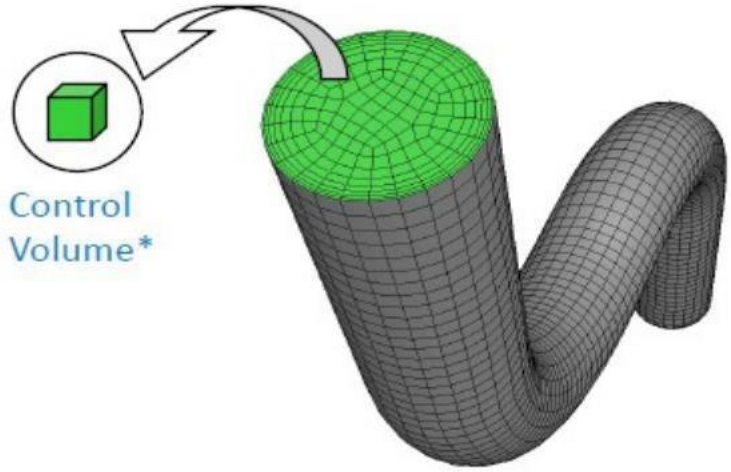

Figure 4.1. Fluid region of pipe flow discretized into finite set of control volumes (mesh) (Google).

4.7. SIMULATION HARDWARE REQUIREMENTS

Considering that simulation computing is a test of the CPU processing power of a computer, we modify the DELL PRECISION TOWER 7910 (Figure 4.2) to deal with this case. The original configuration of this computer including 4 Ghz Fourteen Core E5-2660V4 CPUs; 256GB of ECC DDR4 RAM; 2TB 6Gb/s SATA Solid State Drive; Nvidia Quadro K6000 12GB GDDR5 Graphic Card and Windows 10 Professional 64-Bit Pre-Installed.

The modified one which we use, installed three NVIDIA TITAN RTX graphics cards (Figure 4.3) in parallel to enhance data writing capability. In addition, it replaced E5-2660V4 CPUs to AMD Ryzen Threadripper 2990X 32-Core (Figure 4.4) which is one of the fastest CUP in the market now. What's more, this computer add five Samsung 860

QVO 4TB 2.5 Inch SATA III internal SSD to speed up the reading and writing speed of ANSYS software.

Figure 4.2. DELL PRECISION TOWER 7910 (Google).

Figure 4.3. NVIDIA TITAN RTX graphics card (Google).

Even working with this kind of powerful system, it still cost me 20 hours to run the result of each case.

Figure 4.4. AMD Ryzen Threadripper 2990X 32-Core (Google).

Even working with this kind of powerful system, it still cost me 20 hours to run the result of each case.

5. SIMULATION MODEL BUILD PROCEDURE

5.1. PRE-ANALYSIS

Static settling velocity simulation is a real-world engineering problem numerically using ANSYS FLUENT. I need to remember the size of the experimental model clearly, as well as the initial position where the particles fall, the time which particles fall into the water, and even the initial velocity of the particles entering the water from the air. In this way, I can get more accurate simulation data to compare with the experimental data. Every erroneous data would cause big troubles for simulation calculations. I spend so much time in this step to figure out what kind of experiment data I need in my simulation. The second biggest problem is to find out which boundary condition to use because it will infect my simulation result directly. After doing so many literature reviews and trying so many times, I finally decided to use pressure-far-field as the inlet boundary condition and the pressure out as the outlet boundary condition. This step, called pre-analysis which is indispensable.

5.2. CREATING A FLUENT FLUID FLOW ANALYSIS SYSTEM IN ANSYS WORKBENCH

From the very beginning, I need to start ANSYS Workbench, create a new Fluent fluid flow analysis system, then review the list of files generated by ANSYS Workbench. Workbench can greatly improve my work efficiency in CFD. Later in Workbench, the second create the geometry and later create a mesh and set up a fluid flow analysis for the geometry. Creating a Fluent fluid flow analysis system in ANSYS Workbench shown in Figure 5.1.

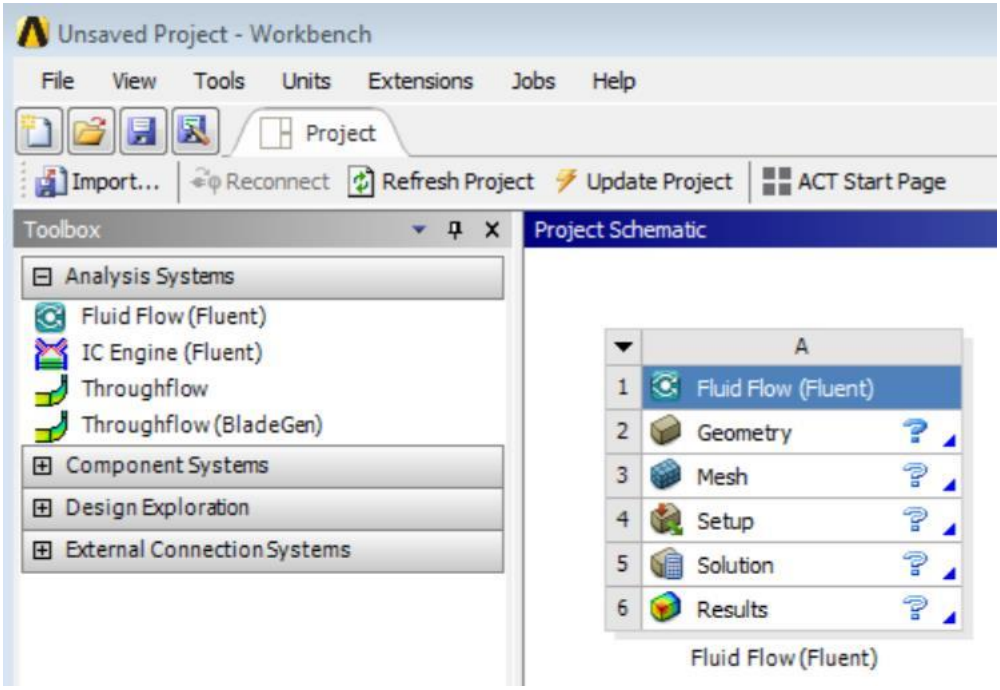

Figure 5.1. Fluent fluid flow analysis system.

5.3. CREATING THE GEOMETRY

In this step, the ANSYS design modeler software can be used. It can also use some other CAD Software such as AutoCAD, Solid works, CATIA, Autocad Inventor etc. I designed my own geometry because there is no suitable geometry file that can be use directly. From the Figure 5.2 shown below, I create a cuboid with a vertical channel inside. The particle will go through the channel to touch the bottom. Then the top of this geometry named as “inlet” and the bottom of the geometry named as “outlet”. Or we can do this step-in meshing since the meshing application provides more comprehensive and extensive named selection functionality.

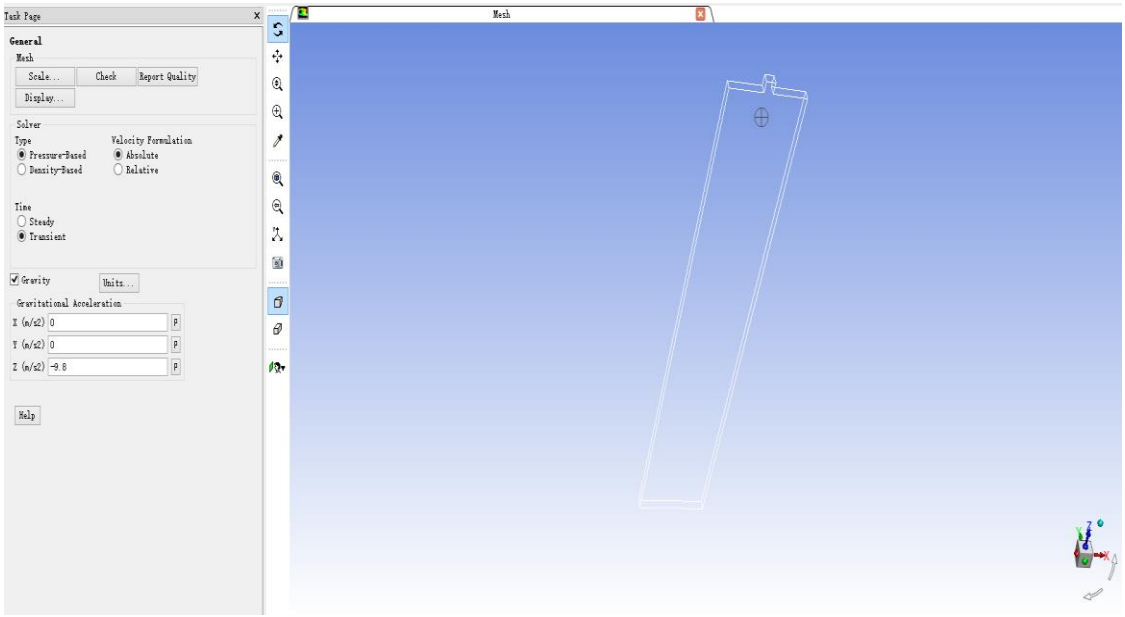

Figure 5.2. Static settling velocity geometry in CFD.

5.4. MESHING THE GEOMETRY IN THE ANSYS MESHING APPLICATION

After creating the geometry, I need to generate a computational mesh throughout the flow volume. Meshing is one of the most important steps for the simulation. Simulation results depend on mesh quality and low-quality mesh can produce poor simulation result, even divergence. Meshing is pre-possessing so I tried so many times to get a perfect meshing plan for my case. For this section, I have to use the ANSYS Meshing application to create a mesh for my CFD analysis, then review the list of files generated by ANSYS Workbench to ensure every step goes well. In order to simplify my work later on in ANSYS Fluent, I label each boundary in the geometry by creating named selections for the cuboid inlets, the outlet, and the symmetry surface. The meshing step shown in the Figure 5.3.

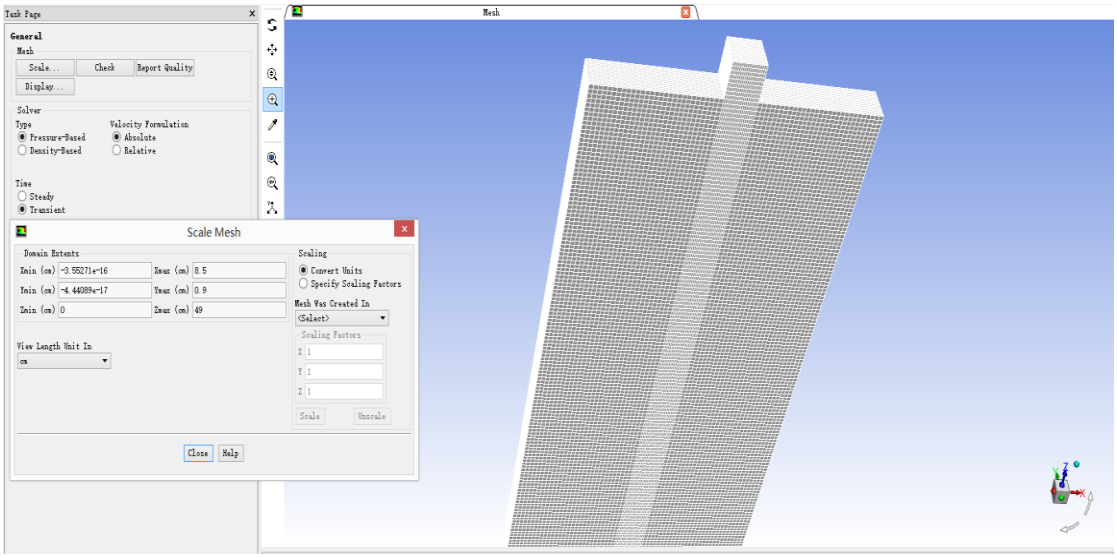

Figure 5.3. Meshing the geometry in CFD.

5.5. PHYSICAL STEP AND NUMERICAL SOLUTION

The finite-volume method is used to directly simulate the motion of the sand particle by the CFD software FLUENT. The fall of sand particle into the water is a complicated process from the aspect of CFD. The existence of water, air and trajectory of sand particle are simulated by volume of fluid (VOF) and discrete phase model (DPM) in FLUENT (Jan Erik OLSEN and Schalk CLOETE, 2009). For the VOF method, the brief theoretical introduction is described as follows. The two-phase fluid behavior can be described by the incompressible Navier-Stokes equation:

$$\rho \frac{\partial \vec{u}}{\partial t} + \rho \nabla \cdot \left(\vec{u}\vec{u} \right) = -\nabla P + \mu \nabla \cdot \left(\nabla \vec{u} + \nabla \vec{u}^{T} \right) + \vec{F} \qquad (2)$$

where $\vec{u}$ is the velocity vector; ρ is the density of fluid; μ is the viscosity of fluid; P is the static pressure; $\vec{F}$ is the general body force, is zero in this study. Only single equation

is solved to obtain the velocity field. In equation (2), the density ρ and viscosity μ are volume-fraction averaged for water and air in each computational cell in this study.

$$\rho = \alpha_a \rho_a + \left(1-\alpha_a\right)\rho_w \tag{3}$$

$$\mu = \alpha_a \mu_a + \left(1-\alpha_a\right)\mu_w \tag{4}$$

where ρ_a and ρ_w are density of air and water, respectively; μ_a and μ_w are viscosity of air and water, respectively. α_a is the volume fraction of air in each cell in this study. In VOF method, only the volumetric fraction of secondary phase is calculated. In this study, the air occupies smaller space, therefore it is set as secondary phase in VOF.

The momentum equation (2) is based on Euler frame of reference. For the motion of sand particle in this study, the discrete phase trajectory is calculated based on Lagrangian reference frame. The particle inertia, hydrodynamic drag, and the force of gravity can all be considered in this model. The trajectory calculation in DPM is based on particle force balance equation:

$$\frac{du_p}{dt} = F_D\left(u-u_p\right) + \frac{g\left(\rho_p-\rho\right)}{\rho_p} + F_a \tag{5}$$

where u_p and u are the velocity of particle and fluid phase, respectively; ρ_p and ρ are the density of particle and fluid phase, respectively; $F_D\left(u-u_p\right)$ is the drag force per unit particle mass; F_a signifies additional force in the particle force balance. For the millimeter scale of sand in this study, F_a is set to zero.

The model geometry is presented in Figure 5.4. The initial contour of volume fraction is presented by colors. As consistent with experimental condition, the height of water level is 45 cm and the length of air regime along z direction is 4 cm. The mesh of geometry is shown in Figure 5.4. Because the sand will drop at the top of container and falls vertically to the bottom of wall. The center region uses finer mesh than other regions. The total mesh in this model is about 670, 000.

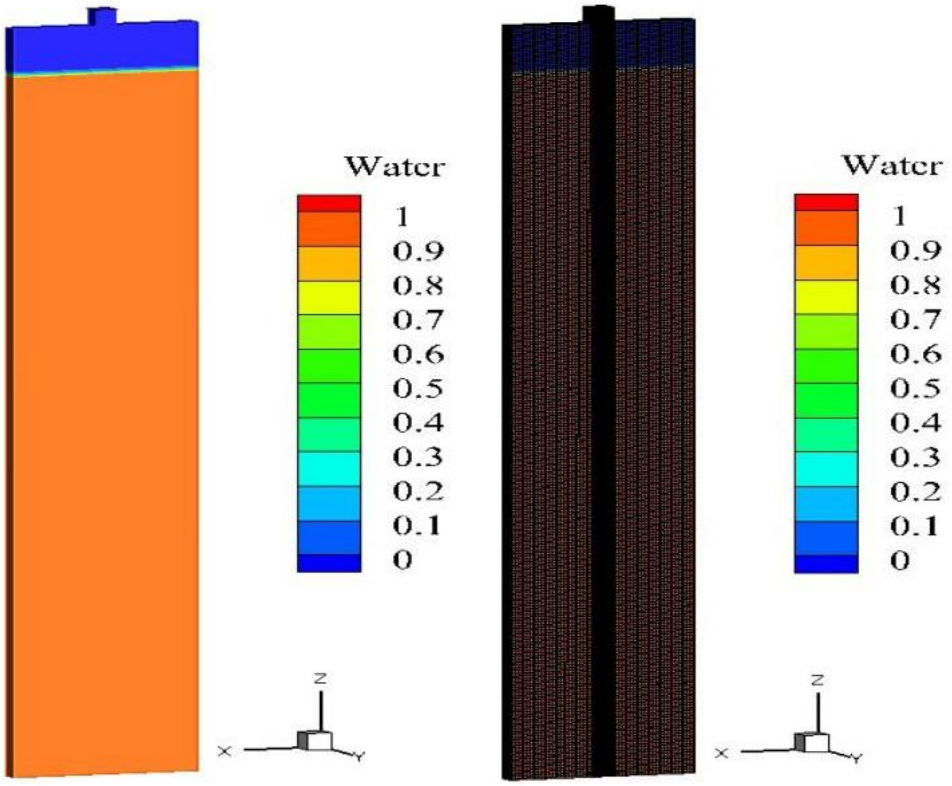

Figure 5.4. The initial contour of volume fraction and the mesh distribution in the geometry.

The sand particle is in the scale of millimeter and has negligible perturbation on the two-fluid system. Therefore, the close boundary condition setting is used in this model. All

boundaries are set as wall in the model. For the DPM boundary, the bottom wall is set as trapped wall boundary and all other wall set as reflected wall boundary. Another consideration for this small particle injection is uncoupled setting of VOF and DPM. It means, the fluid can impose hydrodynamic force on the motion of sand particle, but the motion of particle has no effect on the fluid behavior. This is a reasonable approximation used to reduce the computational burden. More precise tracking of particle force balance and trajectory refers to fictitious domain method [Suckale et al. 2012] and CFD-DEM method [Zhou et al. 2017; Kloss et al. 2012; Moridis et al. 2018]. The transient tracking method and explicit VOF method are used to advance the time steps. The injection point of sand particle is at the center of top boundary, x=4.25 cm, y = 0.45 cm and z = 49 cm. Three types of sand are analyzed with separate diameters of 2 mm, 4 mm and 6 mm. The density of spherical sand used is 2650 kg/m^3.

6. RESULTS AND ANALYSIS

6.1. CFD SIMULATION MODEL VALIDATION

The CFD model is used to simulate the settling process of sand particle in good details. Before that, the model entails validation with experimental data to provide reliable results. As a simple validation, the trajectory of sand particle with diameter 2 mm in water is obtained experimentally. After a good comparison of CFD model and experiments, three cases to analyze effects of fluid types, particle diameters and fracture orientations are accounted for.

6.2. PROPPANT SETTLING VELOCITY VALIDATION

The experimental result is compared with CFD simulation to provide more variability to analyze the settling of sand in fluid. The vertical motion of sand particle is tracked in CFD and experiments. The results are presented in Figure 6.1 as follows. The complete motion of sand particle is shown in Figure 6.1(a). The drop height to the bottom of container is 49 cm. It takes 1.72 seconds and 1.74 seconds for sand particle to settle on the bottom in experiment and CFD respectively. The data has a good agreement on the trajectory and settling time. Because the fluid will pass through the water surface at height of 45 cm, the motion above the water table and below the water table has different drag forces from air and water. The enlargement of motion near the water table is also presented in the Figure 6.1(b). It shows that experimental data is little smaller than that from CFD. This small difference is possibly attributed to the measurement error in the experiment. The time step recording the sand drop is 0.02 s, while the time step set in the FLUENT is

0.005 s. This can also be confirmed by the data number above the water level. The zigzag curve for CFD is due to the time step size. By interpolation of the experimental data, it takes 0.093 s for sand particle to impact the water surface. While it takes 0.095 s in CFD simulation. For the ideal scenario, it would take 0.0904 s for motion of 4 cm in free fall. It infers the small drag in the air domain.

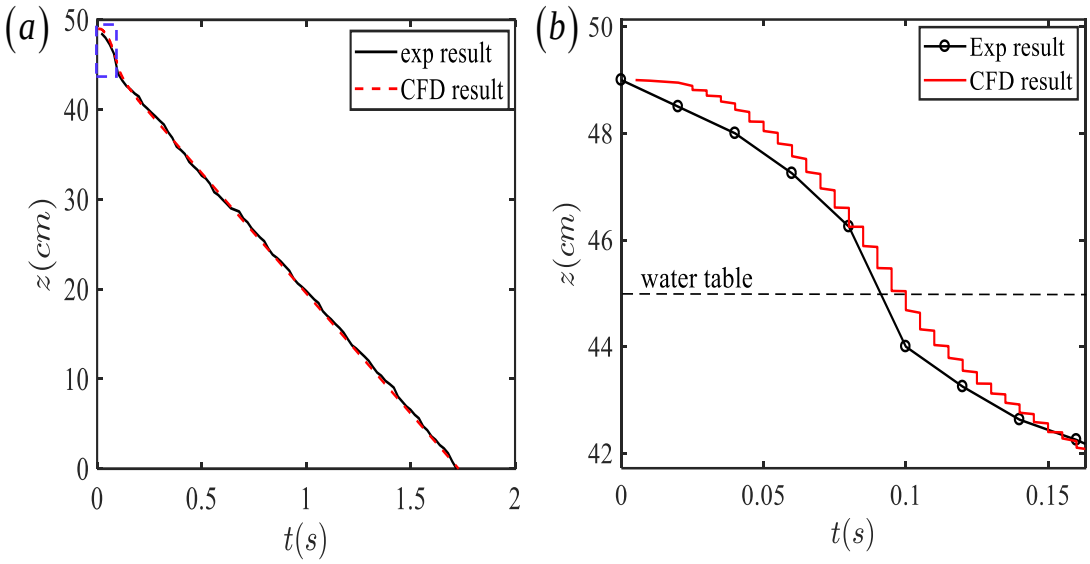

Figure 6.1. The vertical height of sand particle and the enlargement of trajectory near the water table.

The variation of velocity in process of settling from CFD is shown in Figure 6.2. Before 0.095 s, the velocity is linear with respect to time and reaches 88.29 cm/s at water surface. After it drops into the water, the hydraulic drag appreciably increases and leads to decrease of velocity. At 0.345 s, it drops in steady state with velocity of 28.62 cm/s. The steady state velocity in experimental result was 28.7 cm/s. It's noted that CFD result is

based on the empirical drag law and rotational law in DPM setting, while the real case is that the drag and rotation of sand would be different from those empirical laws.

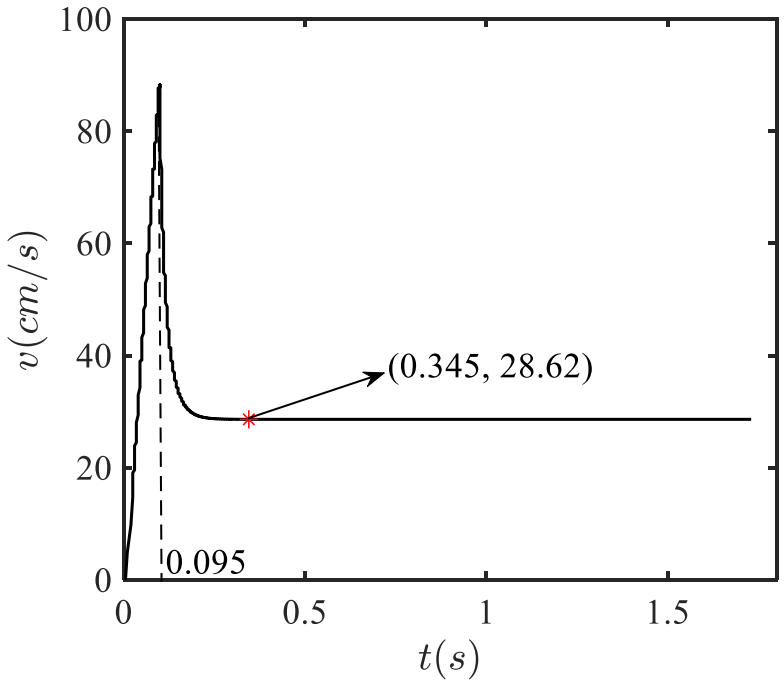

Figure 6.2. The transient velocity of sand particle in settling from CFD simulation. Marker denotes the onset of steady state.

This is one possible reason to cause the simulation error. More accurate characterization of drag and rotation of sand particle is necessary to capture the motion of sand. In addition, the uncoupling setting of DPM and VOF would also cause some error in the simulation.

6.3. FRACTURE FLUID RHEOLOGY VALIDATION

Water is the default faucet water with standard properties. HVFR, a fluid widely used to deliver proppant in fracture. Linear gel has the same capability to deliver proppant in fracture. Water, as a Newton fluid, has constant viscosity of 0.001 Pa·s. HVFR, as a non-Newton fluid, has varying viscosity at different shear rate. The rheological properties of HVFR was measured in atmosphere condition using advanced rheometer. The variation of viscosity with shear rate is presented in Figure 6.3. This experimental curve is fitted by non-Newton power law. The power law used in the simulation for HVFR is:

$$\eta = 0.51062\dot{\gamma}^{-0.6633} \tag{6}$$

The power law for linear gel is:

$$\eta = 0.18802\dot{\gamma}^{-0.4121} \tag{7}$$

where η is the apparent or effective viscosity; $\dot{\gamma}$ is the shear rate. The flow consistency index and flow behavior index can be set by these fitting equations in simulation. The error induced by fitting will inevitably be introduced into the final settling parameters. This effect on the final results will be analyzed later.

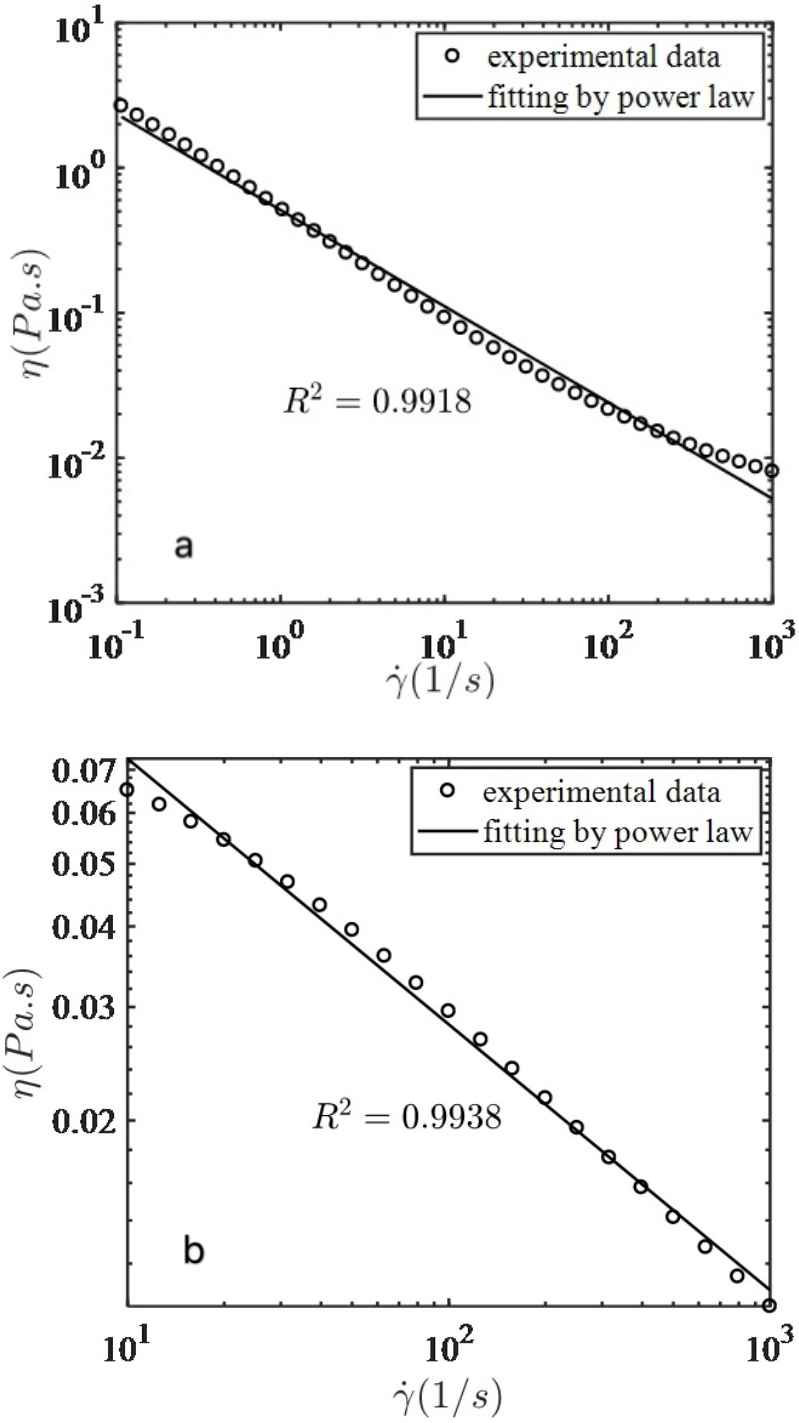

Figure 6.3.Variation of viscosity η with shear rate $\dot{\gamma}$ and fitting by non-Newton power law for (a) HVFR and (b) linear gel. The fitting equation for HVFR is $\eta = 0.51062\dot{\gamma}^{-0.6633}$ and $\eta = 0.18802\dot{\gamma}^{-0.4121}$ for linear gel.

7. SENSITIVITY ANALYSE

After validation of CFD model by dropping of sand particle in water, it's reliable to extend this analysis for fracture fluid and other pumping conditions. In fracture, the proppant transport is affected by the fluid type, proppant size, fracture orientation, etc. In this study, the effect of fluid type, proppant size and fracture orientation on the settling of proppant is analyzed in this section. The complete analysis is summarized in the Table 7.1.

Table 7.1. The summary of analysis in this study.

Case number	Fluid type	Proppant diameter	Fracture orientation
I	Water	2 mm	90°
	HVFR		
	Linear gel		
II	HVFR	2 mm	90°
		4 mm	
		6 mm	
III	HVFR	2 mm	90°
			60°
			45°

When the dip angle of fracture orientation is large, the sand would reflect on the boundary wall and then slide along the wall to the bottom. The interaction of proppant with the fracture surface is of essential interest to understand the settling and finally spatial

distribution of proppant. Three orientations with dig angles of 90°, 60° and 45° are considered. The sketch for these fracture orientations is shown in Figure 7.1.

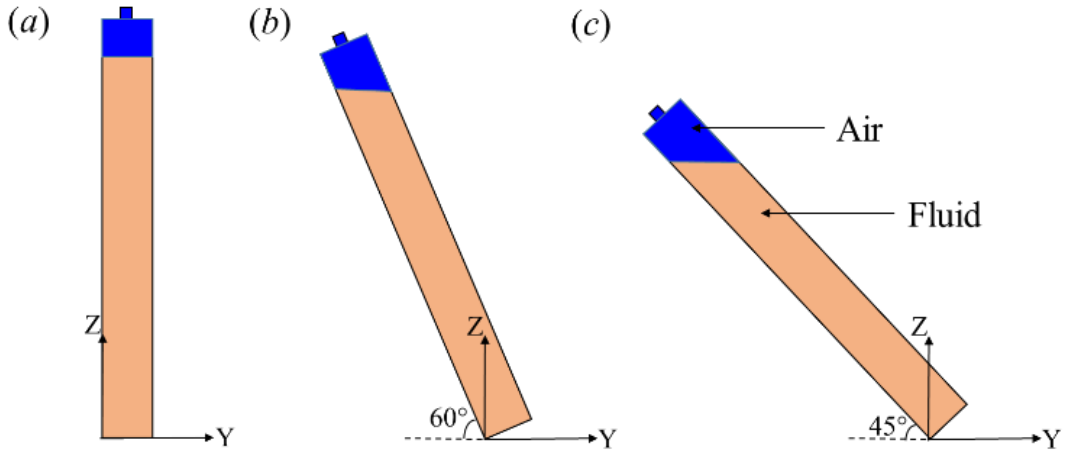

Figure 7.1. Side views of fracture orientations at (a) 90°, (b) 60° and (c) 45°. The 3D coordinate view corresponds to geometry display in Figure 5.4.

7.1. CASE I: EFFECT OF FLUID TYPES

The effect of water, HVFR and linear gel on the settling of proppant is analyzed as case I study. The proppant used is in a diameter of 2 mm and the fracture is vertical oriented. The vertical distance to bottom of container is tracked in Figure 7.2. It takes 1.74 s, 13.38 s and 333.78 s for same sand particle to deposit on the bottom when using water, linear gel, and HVFR, respectively. It indicates higher resistive capability of HVFR to oppose the drop of sand particle. This can also be confirmed from the rheology property presented in Figure 6.3. The transient velocity of proppant is shown in Figure 7.3. Before falling into the water region, the velocity is linear function of time. At the moment that proppant enters into the water region, it takes less time for HVFR to decelerate to steady state. It also vilifies the high resistive capability of HVFR to other two types of fluid.

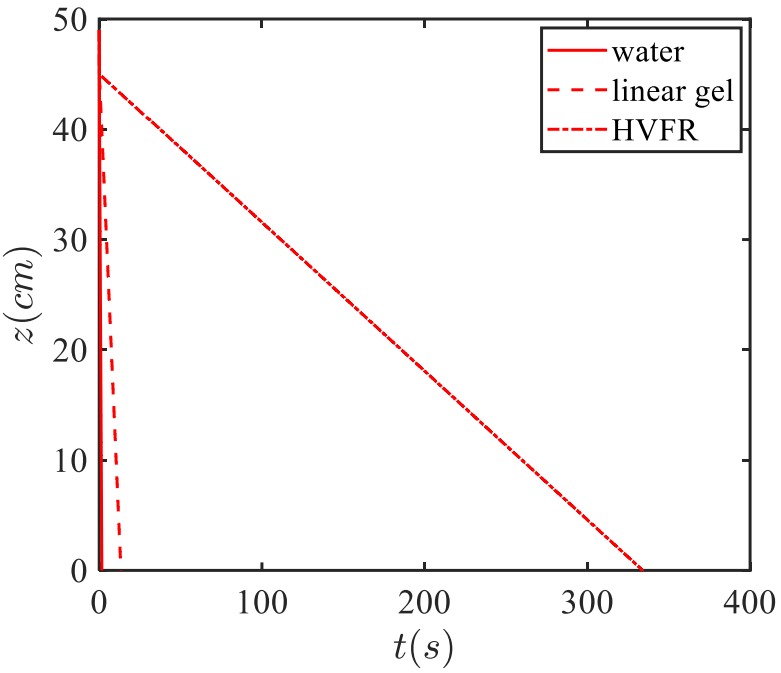

Figure 7.2. The height of sand particle of 2 mm in three types of fluid.

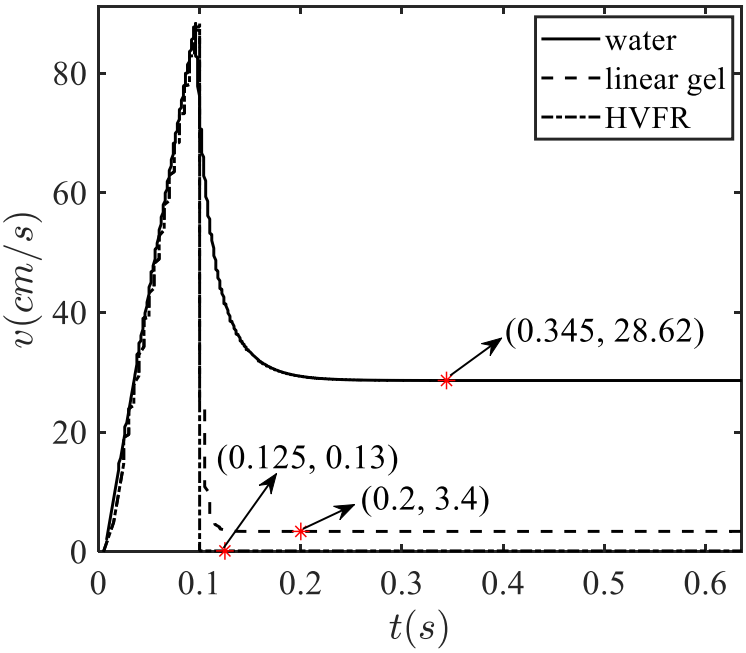

Figure 7.3. The transient velocity of proppant with 2 mm in three types of fluid. Only small-time range are presented for better illustration. Three red markers denote the onset of steady states.

The steady-state falling velocity of proppant in water, linear gel and HVFR are 28.62 cm/s, 3.4 cm/s and 0.13 cm/s, respectively.

7.2. CASE II: THE EFFECT OF PROPPANT SIZE

In the process of falling, single proppant is mainly subjected to drag force and gravitational force as shown in equation (5). As the larger size of proppant, the gravitational force and drag force increase concurrently. Due to the opposite force direction, the net force on the settling proppant is of key interest to analyze. In addition, different sizes of proppant are used in the petroleum industry. The effect of proppant size on the finally spatial distribution in hydraulic fracture is of significant application. Therefore, different proppant sizes are used in this section to investigate their significance to settling velocity.

The vertical distance to bottom is tracked in the settling process as shown in Figure 7.4. It takes 333.78 s, 83.50 s and 37.09 s to deposit on the bottom for proppant with diameter 2 mm, 4 mm and 6 mm, respectively. It shows that larger proppant takes less time to settle down. It alludes that the gravitational force overrides the drag force from aspect of proppant size.

The transient velocity of proppant is plotted in Figure 7.5. Only small range of time is presented for better illustration. It's noted that the zigzag curve is attributed to the time steps setting in the simulation. The time step size is 0.005 s. After incorporating this difference by time step size, the velocities for three different diameters are almost the same before the abrupt jumping of velocity around 0.1 s. The steady state time for proppant with D=4 mm and 6 mm are almost the same after considering the error from time step size.

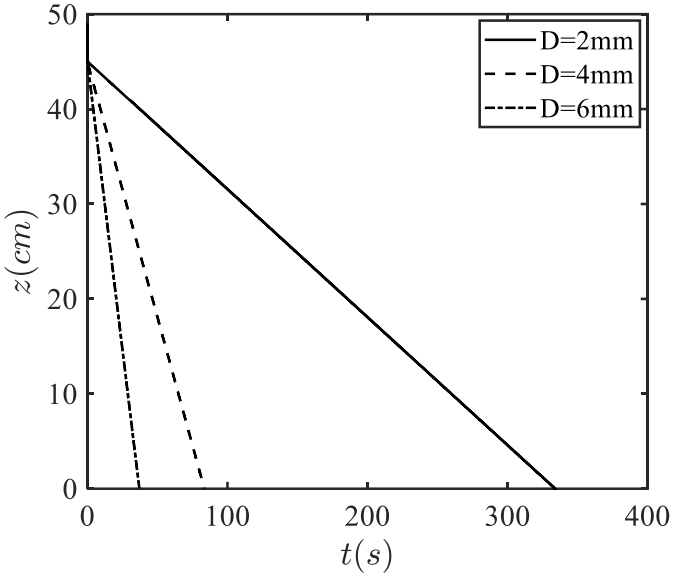

Figure 7.4. The height of proppant of three diameters (D=2 mm, 4 mm and 6 mm) in HVFR.

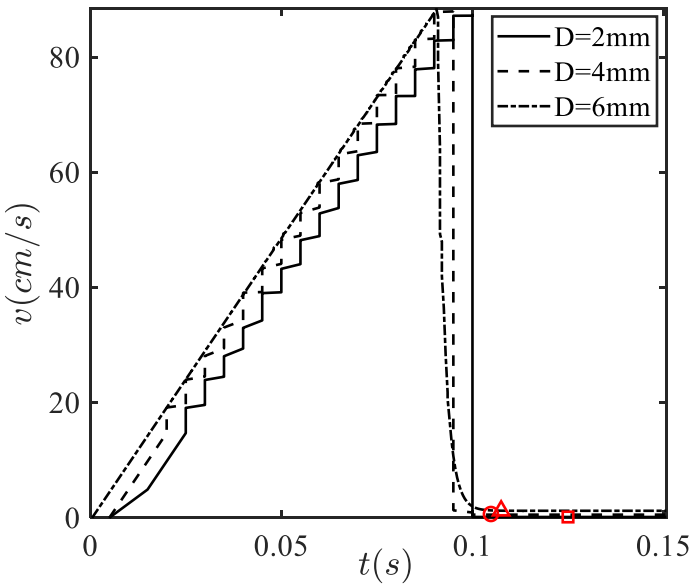

Figure 7.5. The transient velocity of proppant with diameters 2 mm, 4 mm and 6 mm in HVFR. Only small-time range are presented for better illustration. Three red markers denote the onset of steady states: red box corresponds to point (0.125, 0.13) for D=2 mm; red circle corresponds to point (0.105, 0.54) for D=4 mm; red upper triangle corresponds to point (0.108, 1.23) for D=6 mm.

Whereas, it takes longer for proppant with D=2 mm to become steady, about 0.125 s. But this value is still very close to those of D=4 mm and 6 mm. It infers the small influence of proppant size on time to reach steady state for proppant. However, the steady-state velocities have more difference. They are 0.13 cm/s, 0.54 cm/s and 1.23 cm/s for proppants with D=2 mm, 4 mm and 6 mm, respectively.

7.3. CASE III: THE EFFECT OF FRACTURE ORIENTATION

For the vertical fracture in preceding sections, the drag force is from fluid. When the fracture is orientated at certain angle, the proppant would fall on the boundary wall and then slide to the bottom. The collision and sliding on the wall provide much larger drags for proppant falling. The fracture orientation is hence analyzed in this section to understand the motion of proppant. Three dip angles are considered: 45°, 60° and 90° as shown in sketches in Figure 7.2. The container keeps the same but when orientated, the falling height of proppant with respect to origin changed. For 45°, 60° and 90°, the initial falling heights are 34.95 cm, 42.66 cm and 49 cm, respectively. The distances of proppant falling in air are also different for these angles. The heights of proppant are shown in Figure 7.6. For orientation of 45°, proppant stops on the tilted wall at 31 cm. For orientations of 60° and 90°, proppant falls into water at 39 cm and 45 cm, respectively. Then, it slides along the wall at different magnitudes of velocity for orientation of 60° and 90°. Figure 7.7 shows the transient velocity of proppant in fracture with different orientations angles. The steady-state velocities are 0 cm/s, 0.11 cm/s and 0.13 cm/s for orientations of 45°, 60° and 90°, respectively.

The boundary wall is slippery boundary without roughness. However, the real fracture surface is rough and wavy [Chao and Deng, 2018; Chao et al. 2018]. When the proppant is pumped into the open tilted fracture, the friction of proppant with rough fracture is much larger than that in this study. The proppant is likely to be trapped at the rough fracture surface. To incorporate this effect, the roughness of fracture will be considered on the motion of proppant in our next work.

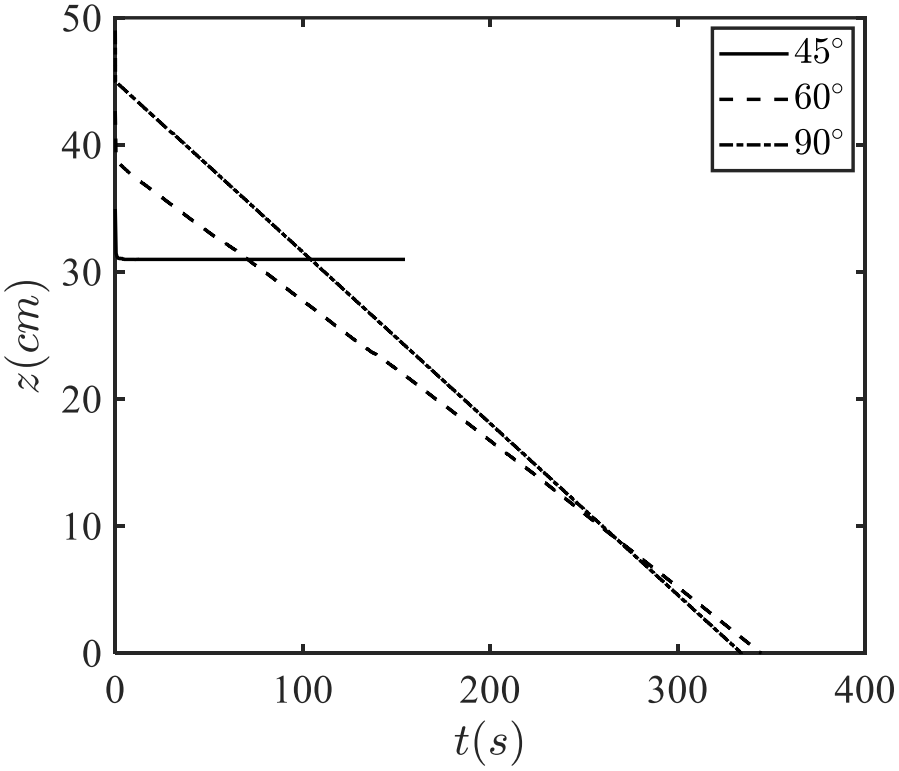

Figure 7.6. The transient height of proppant of diameter 2 mm in HVFR with different fracture orientations (45° and 60° and 90°). The short line for 45° orientation denotes the proppant stopping on the tilted wall.

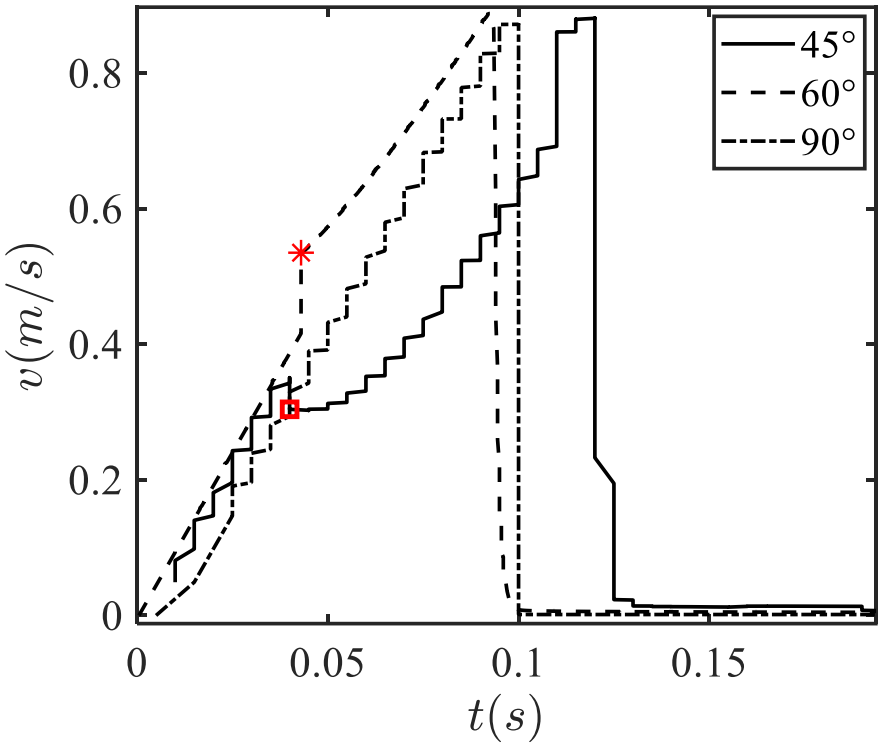

Figure 7.7. The transient velocity of proppant of diameter 2 mm in HVFR with different fracture orientations (45° and 60° and 90°). The red markers denote the instants that proppant strikes boundary wall.

8. CONCLUSION

Integrated work between experimental results and simulation output were investigated to predict the proppant settling velocity in HVFRs. Proppant settling velocity behavior was also studies at different fracturing fluids, proppant sizes, and fracture orientation. Both studies reveal reduction motion during particle settling. This reduction depends on fluid rheology and fracture orientation degree. In case I, the steady-state falling velocity of proppant in water, linear gel and HVFR are 28.62 cm/s, 3.4 cm/s and 0.13 cm/s, respectively. In case II, the steady state time for proppant with D=4 mm and 6 mm are almost the same after considering the error from time step size. Whereas, it takes longer for proppant with D=2 mm to become steady. In case III, the results show that the collision and sliding on the wall provide much larger drags for proppant falling.

9. FUTURE WORK AND RECOMMENDATIONS

In this study, the effect of fluid type, proppant size and fracture orientation on the settling of proppant is analyzed for three cases. Actually, it can be analyzed to 27 different results. This work can be down in the future to make the results more comprehensive. In addition, settling velocity experiment result using HVFR can be analyzed and compared with simulation result to make the validation part perfectly.

The recommended study for static settling velocity experiment is to use the real proppant instead of the particles in this study, if it possible. What's more, the real-world experiment fracture is also expected.

REFERENCES

Al-Muntasheri, G. A. 2014. A Critical Review of Hydraulic Fracturing Fluids over the Last Decade. Society of Petroleum Engineers. doi:10.2118/169552-MS.

Ba Geri, M., Imqam, A., Bogdan and Shen, L. 2019. Investigate the Rheological Behavior of High Viscosity Friction Reducer Fracture Fluid and Its impact on Proppant Static Settling Velocity. Society of Petroleum Engineers.

Beckwith Robin. 2012. Depending on Guar- For Shale Oil and Gas Development, Journal of Petroleum Technology, December (2012)., 44-55.

Christoph Kloss, Christoph Goniva and Alice Hager. 2012. Models, Algorithms and Validation for Opensource DEM and CFD-DEM. Progress in Computational Fluid Dynamics.

Carl Aften, Solvay S. A. and Flotek Chemistry LLC. 2018. Analysis of Various High Viscosity Friction Reducers and Brine Ranges Effectiveness on Proppant Transport. Society of Petroleum Engineers.

C. S. Peskin, "Numerical analysis of blood flow in the heart," Journal of Computational Physics, vol. 25, no. 3, pp. 220–252, 1977.

Dahlgren, K., Green, B., Williams, B., Inscore, J., Domelen, M. V and Fenton, A. 2018. Case Studies of High Viscosity Friction Reducers HVFR in the STACK Play. Society of Petroleum Engineers.

ENGEBRETSEN, T., NORTHUG, T., SJØEN, K., and FANNELØP, T.K. (1997), "Surface flow and gas dispersion from a subsea release of natural gas.", Seventh Int. Offshore and Polar Engineering Conference, Honolulu, USA. Economides, M.; Nolte, K. Reservoir Stimulation, NY and Chichester, 3rd ed. Wiley, 2000.

G. Pianet a and E. Arquis. 2007. Simulation of particles in fluid: a two-dimensional benchmark for a cylinder settling in a wall-bounded box. European Journal of Mechanics B/Fluids 27 (2008) 309–321.

Gandossi, L. 2013. An Overview of Hydraulic Fracturing and Other Formation Stimulation Technologies for Shale Gas Production. Report by the Joint Research Centre of the European Commision. doi: 10.2790/99937.

Hu, Y. T., Fisher, D., Kurian, P and Calaway, R. (2018, January 23). Proppant Transport by a High Viscosity Friction Reducer. Society of Petroleum Engineers.

Haiyan Zhao, Samuel Danican and Hortencia Torres. 2018. Viscous Slickwater as Enabler for Improved Hydraulic Fracturing Design in Unconventional Reservoirs. Society of Petroleum Engineers.

Jan Erik OLSEN and Schalk CLOETE. 2009. Coupled DPM and VOF Model for Analyses of Gas Stirred Ladles at Higher Gas Rates. Seventh International Conference on CFD in the Minerals and Process Industries CSIRO, Melbourne, Australia.

Jennings, A.R. 1996. Fracturing Fluids - Then and Now. Journal of Petroleum Technology 48 (7): 604-610.

Jenny Suckale, James A. Sethian, Jiun-der Yu, and Linda T. Elkins-Tanton. 2012. Direct Numerical Simulations of Crystal Settling in Nondilute Magmatic Suspensions. Journal of Geophysical Research.

James Feng, Howard H. Hu and Daniel D. Joseph. 1994. Direct Simulation of Initial Value Problems for the Motion of Solid Bodies in a Newtonian Fluid Part1. Sedimentation. University of Pennsylvania ScholarlyCommons.

J. Ding, D. Gidaspow, A bubbling fluidization model using kinetic theory of granular flow, AIChE J. 36 (1990) 523–538.

Kyle Dahlgren, Brett Green, Brandon Williams, and Josh Inscore. Case Studies of High Viscosity Friction Reducers HVFR in the STACK Play. Society of Petroleum Engineers.

Kanarska Y, Lomov I, Antoun T (2011) Mesoscale simulations of particulate flows with parallel distributed lagrange multiplier technique. Comput Fluids 48(1):16–29

Ling Zhou, Lingjie Zhang and Ling Bai, 2017. Experimental study and transient CFD/DEM simulation in a fluidized bed based on different drag models. RSC Advances.

Lingjuan Shen, Leonid Vigderman and David Heller. 2018. Can Friction Reducers Transport Sand During Fracturing Treatment? Society of Petroleum Engineers.

Lianping Wang and Martin M. 1993. Settling velocity and concentration distribution of heavy particles in homogeneous isotropic turbulence. J. Fluid Mech. (1993), vol. 256, pp. 21-68.

Liu, Y., & Sharma, M. M. 2005. Effect of Fracture Width and Fluid Rheology on Proppant Settling and Retardation: An Experimental Study. Society of Petroleum Engineers. doi:10.2118/96208-MS.

L. Wang, Z.L. Guo and J.C. Mia. 2014. Drafting, kissing and tumbling process of two particles with different sizes. 2014 Elsevier Ltd.

Motiee, M., Johnson, M., Ward, B., Gradl, C., McKimmy and Meeheib, J. 2016. High Concentration Polyacrylamide-Based Friction Reducer Used as a Direct Substitute for Guar-Based Borate Crosslinked Fluid in Fracturing Operations. Society of Petroleum Engineers.

Mohanty, K. K., and Ming Gu, A. G. 2012. "Improvement of Fracturing for Gas Shales. "Report for RPSEA (Research Partnership to Secure Energy for America).

Mark Van Domelen and Wayne Cutrer. 2017. Applications of Viscosity-Building Friction Reducers as Fracturing Fluids. Society of Petroleum Engineers.

Matt Johnson and Producers Service Corporation. 2018. Successful Implementation of High Viscosity Friction Reducer in Marcellus Shale Stimulation. Society of Petroleum Engineers.

Machac, I. and Lecjaks, Z. 1995. Wall Effect for a Sphere Falling Through a Non-Newtonian Fluid in a Rectangular Duct. Chem. Eng. Sci. 50 (1): 143-148.

Malhotra, S. and Sharma, M.M. 2012. Settling of Spherical Particles in Unbounded and Confined Surfactant-Based Shear Thinning Viscoelastic Fluids: AnExperimental Study. Chemical Engineering Science 84: 646-655.

M. Xu, F. Chen, X. Liu, W. Ge, J. Li, Discrete particle simulation of gas–solid two-phase flows with multi-scale CPU-GPU hybrid computation, Chem. Eng. J. 207 (2012)746–757.

Pratanu Roy and Wyatt L. Du Frane. 2016. Numerical and Experimental Studies of Particle Settling in Real Fracture Geometries. Rock Mech Rock Eng (2016) 49:4557–4569.

Patankar NA, Singh P, Joseph DD, Glowinski R, Pan TW (2000) A new formulation of the distributed lagrange multiplier/fictitious domain method for particulate flows. Int J Multiph Flow 26(9):1509–1524

Plimpton S., Fast Parallel Algorithms for Short-Range Molecular Dynamics, J Comp Phys, 117, 1–19 (1995) Sahai, R., Miskimins, J. L., & Olson, K. E. (2014, February 4). Laboratory Results of Proppant Transport in Complex Fracture Systems. Society of Petroleum Engineers. doi:10.2118/168579-MS

Phani B. Gadde, Yajun Liu and Jay Norman. 2004. Modeling Proppant Settling in Water-Fracs. Society of Petroleum Engineers.

Palisch, T. T., Vincent, M., & Handren, P. J. 2010. Slickwater Fracturing: Food for Thought. Society of Petroleum Engineers. doi:10.2118/115766-PA.

R. Kou, G. J. Moridis, and T. A. Blasingame, Texas A&M University. 2018. Analysis and Modeling of Proppant Transport in Inclined Hydraulic Fractures. Society of Petroleum Engineers.

S. Glowinski, T.-W. Pan, T. I. Hesla, and D. D. Joseph, "A distributed Lagrange multiplier/fictitious domain method for particulate flows," International Journal of Multiphase Flow, vol.25, no. 5, pp. 755–794, 1999.

Rongqian Chen, Yi Liu, and Deming Nie. 2017. Computer Simulation of Three Particles Sedimentation in a Narrow Channel. Mathematical Problems in Engineering, Hindawi.

Robert, M., and Pin, T. J. Enzyme Breaker for Galactomannan Based Fracturing Fluid. USA Patent 5201370, 13 April 1993.

Stephen Drylie and Robert Duenckel. 2018. An Investigation of Proppant Transport in Friction Reducer Fluid Systems Utilizing a Large Slot Flow Apparatus. Society of Petroleum Engineers.

Van Domelen, M., Cutrer, W., Collins, S and Ruegamer, M. 2017. Applications of Viscosity-Building Friction Reducers as Fracturing Fluids. Society of Petroleum Engineers.

Weaver, J., Schmelzl, E., Jamieson, M., and Schiffner, G. New Fluid Technology Allows Fracturing without Internal Breakers, in SPE Gas Technology Symposium, Calgary, 2002.

Xizhong Chen and Junwu Wang. 2014. A comparison of two-fluid model, dense discrete particle model and CFD-DEM method for modeling impinging gas-solid flows. 2014 Elsevier B.V.

X.-Z. Chen, D.-P. Shi, X. Gao, Z.-H. Luo, A fundamental CFD study of the gas–solid flow field in fluidized bed polymerization reactors, Powder Technol. 205 (2011)276–288.

Y. Thomas Hu, David Fisher, and Pious Kurian. 2017. Proppant Transport by a High Viscosity Friction Reducer. Society of Petroleum Engineers.

Zhenhua Xia, Kevin W. Connington and Saikiran Rapaka. 2009. Flow patterns in the sedimentation of an elliptical particle. J. Fluid Mech. (2009), vol. 625, pp. 249–272.

Y. Tsuji, T. Kawaguchi, T. Tanaka, Discrete particle simulation of two-dimensional fluidized bed, Powder Technol. 77 (1993) 79–87.

Zeng C., Deng W., Wu C. 2018. Thermal Stress Effect on Fracture Integrity in Enhanced Geothermal Systems. In: Zhang L., Goncalves da Silva B., Zhao C. (eds) Proceedings of GeoShanghai 2018 International Conference: Rock Mechanics and Rock Engineering. GSIC 2018. Springer, Singapore.

Zeng, C and Deng, W. 2018. The Effect of Radial Cracking on the Integrity of Asperity under Thermal Cooling Process. American Rock Mechanics Association.

VITA

Chen Yuan was born in Xian, China. He received his bachelor's degree in Geological Engineering from Xian Shiyou University in June 2017. He joined Missouri University of Science and Technology in August 2017. He joined hydraulic fracturing research group under direct supervision of Dr. Abdulmohsin Imqam. He received his master's degree in Petroleum Engineering in May 2019 from Missouri University of Science and Technology.